Fossil Record 28 (1) 2025, 17–43 | DOI 10.3897/fr.28.131671

PENSOFT

für Natur MUSEUM FÜR NATURKUNDE BERLIN

A new *Archaeopteryx* from the lower Tithonian Mörnsheim Formation at Mühlheim (Late Jurassic)

Christian Foth[1,2], Thomas van de Kamp[3,4], Helmut Tischlinger[5], Theron Kantelis[6], Ryan M. Carney[6], Marcus Zuber[3], Elias Hamann[3], Jonathan J. W. Wallaard[7], Norbert Lenz[8], Oliver W. M. Rauhut[9,10,11], Eberhard Frey[12]

1 *Department of Geosciences, University of Fribourg, Ch. du Musée 6 1700 Fribourg, Switzerland*
2 *Institut für Biowissenschaften, Allgemeine und Spezielle Zoologie, Universität Rostock, Universitätsplatz 2, 18055 Rostock, Germany*
3 *Institute for Photon Science and Synchrotron Radiation (IPS), Karlsruhe Institute of Technology (KIT), Hermann-von-Helmholtz-Platz 1, 76344 Eggenstein-Leopoldshafen, Germany*
4 *Laboratory for Applications of Synchrotron Radiation (LAS), Karlsruhe Institute of Technology (KIT), Kaiserstraße 12, 76131 Karlsruhe, Germany*
5 *Jura-Museum Eichstätt, Willibaldsburg, 85072 Eichstätt, Germany*
6 *Department of Integrative Biology, University of South Florida, Tampa, Florida, 33620 USA*
7 *Oertijdmuseum, Bosscheweg 80, 5383 WB Boxtel, Netherlands*
8 *Auf dem Guggelensberg 14, 76227 Karlsruhe, Germany*
9 *Staatliche naturwissenschaftliche Sammlungen Bayerns (SNSB), Bayerische Staatssammlung für Paläontologie und Geologie, Richard-Wagner-Straße 10, 80333 München, Germany*
10 *Department for Earth and Environmental Sciences, Sektion Palaeontology and Geobiology, Ludwig-Maximilians-Universität, Richard-Wagner-Str. 10, 80333 München, Germany*
11 *GeoBioCenter, Ludwig-Maximilians-Universität, Richard-Wagner-Straße 10, 80333 München, Germany*
12 *Sonnenbergstraße 27, 75180 Pforzheim, Germany*

https://zoobank.org/ACD10500-809C-4BB7-8A44-11B7D4E622B6

Corresponding author: Christian Foth (christian.foth@gmx.net)

Academic editor: Florian Witzmann ♦ **Received** 9 July 2024 ♦ **Accepted** 21 October 2024 ♦ **Published** 3 January 2025

Abstract

Here we describe a new specimen of *Archaeopteryx* sp. from the lower Tithonian Mörnsheim Formation in the Franconian Alb of Bavaria, Germany. This fossil is the third avialan specimen found in this formation. The skeleton comprises the right forelimb and shoulder as well as fragments of the left forelimb and both hind limbs. The lengths of the humerus and ulna are most similar to those of the Munich specimen of *Archaeopteryx*. Despite the specimen having been massively altered by late diagenesis, it can be referred to *Archaeopteryx* sp., based on the morphology of the furcula, coracoid, humerus and radius, as well as a manual ungual, which nests within the morphospace of *Archaeopteryx* rather than that of *Anchiornis*. Phylogenetic analyses also support the assignment of the new specimen to *Archaeopteryx*. Due to the fossil's state of preservation, as well as the still-unresolved taxonomy of the genus *Archaeopteryx* on the species level, an identification beyond genus remains impossible.

Key Words

Archaeopteryx, Avialae, Late Jurassic, origin of birds, tomography, taphonomy

Introduction

The laminated limestones of the Franconian Alb in Bavaria, southern Germany, are world-famous for their numerous exceptionally preserved fossils (see Arratia et al. (2015) for a summary). Most fossils reported from this limestone come from quarries in the Altmühltal Formation (*sensu* Niebuhr and Pürner (2014)). However, in recent years, an increasing abundance of fossils have also become known from the underlying Torleite Formation and the overlying Mörnsheim Formation (see, for example, Tischlinger (2001); Viohl and Zapp (2007); Heyng et al. (2011, 2015); Rauhut et al. (2019)). More excavation activities in these units, especially at the localities of Schamhaupten and Painten and in the layers cropping out in the Schaudiberg quarry near Mühlheim within the Mörnsheim Formation, have revealed that, in places, these formations appear to be more fossiliferous than the Altmühltal Formation itself (see, for example, Viohl and Zapp (2007); Heyng et al. (2011); Heyng et al. (2015); Albersdörfer and Häckel (2015); Rauhut et al. (2019); Wallaard et al. (2021)).

The arguably historically most important and debated fossil taxon from the Franconian laminated limestones is *Archaeopteryx*, which has played a crucial role in the controversy about the theory of evolution in general and the origin of birds in particular (for example, Huxley (1868); Heilmann (1926); Ostrom (1976); Wellnhofer (2009)). This taxon to date is only known from the lower Tithonian of Bavaria, Germany, with nine out of eleven specimens currently referred to this genus having been unearthed from the Altmühltal Formation (Rauhut et al. 2018, 2019). Only one specimen, the Schamhaupten specimen (see comments on the naming of specimens below), comes from the Kimmeridgian/Tithonian boundary in the lowermost part of the Painten Formation (Rauhut et al. 2018). Another single and fragmentary skeleton, the Daiting specimen, comes from the Mörnsheim Formation that overlies the Altmühltal Formation (Mäuser 1997; Tischlinger 2009) and has been referred to as a putatively new species, *Archaeopteryx albersdoerferi* Kundrát et al., 2019. According to what is known from the fossil record, the genus *Archaeopteryx* existed over a range of at least ~ 64 km (Rauhut et al. 2019) and for a timespan of at least between 700,000 and one million years (cf. at least five million years each for *Confuciusornis sanctus* and *Sapeornis chaoyangensis* (Chiappe and Meng 2016; Wang et al. 2019a)). Morphological variations (for example, dentition and limb proportions) within the genus suggest that *Archaeopteryx* underwent evolutionary changes and may have split into different species throughout this time (Rauhut et al. 2018).

For more than 150 years, the genus *Archaeopteryx* was the only Jurassic representative referable to Paraves, a theropod clade that includes birds (Avialae *sensu* Gauthier 1986) and their closest relatives, dromaeosaurids and troodontids (for example, Sereno (1999); Clark et al. (2002); Xu et al. (2011); Turner et al. (2012)). The discovery of a diverse assemblage of paravian theropods from slightly older rocks in northeast China during the last decades (for example, Xu et al. (2009, 2011); Lefèvre et al. (2017); Hu et al. (2018); Xu et al. (2023)); the identification of the fragmentary "Haarlem specimen of *Archaeopteryx*" as a separate taxon, *Ostromia crassipes* (Meyer, 1857), belonging to another clade of paravians, the Anchiornithinae (*sensu* Xu et al. (2016)) (Foth and Rauhut 2017); and the discovery of *Alcmonavis poeschli* Rauhut et al., 2019, in the Schaudiberg quarry, which is morphologically more derived than *Archaeopteryx* (Rauhut et al. 2019), revealed a hitherto unexpected complexity of paravian evolution, diversity and distribution during the Late Jurassic.

The new "Urvogel" specimen from the Lower Tithonian Mörnsheim Formation at Mühlheim described herein is the second theropod reported from there, the third from the Lower Tithonian Mörnsheim Formation and the 14th overall (Rauhut et al. 2019). Here, we define "Urvogel" (German for "first bird"; plural "Urvögel") as any paravian from the Late Jurassic Franconian Alb. This general definition accommodates all past and future taxonomic interpretations of these specimens (paraphyletic vs. monophyletic; interfamilial vs. conspecific). It should be noted that a lack of consensus abounds within the specialist community, even amongst the authors of this paper. For example, some authors herein consider the known Urvögel to most likely represent a monophyletic group of at least a congeneric *Archaeopteryx* growth series, with some key characters exhibiting artefacts of taphonomy (interpretation followed by RMC and TK; Carney et al. (2020)). Ultimately, a detailed taxonomic study of all Urvögel specimens is necessary.

Geological and palaeontological context

The Mörnsheim Formation forms part of the southern German Weißjura Group that consists of mainly calcareous marine sediments that abundantly outcrop in Bavaria and Baden-Württemberg and was deposited on an extensive carbonate platform along the northern margin of the Tethyan Ocean that extended from Germany to southern France in the Late Jurassic (Keupp et al. 2007; Viohl 2015). In the southern Franconian Alb, Bavaria, the Weißjura Group in the region between Weißenburg and Regensburg is famous for partially laminated, partially silty limestones of late Kimmeridgian to early Tithonian age, commonly referred to as the "Solnhofen limestone". For the lithostratigraphy, we refer to the nomenclature and correlations of the formations proposed by Niebuhr and Pürner (2014). Accordingly, the "Solnhofen limestone" *sensu stricto* is part of the Altmühltal Formation and restricted to the area northwest of Ingolstadt, whereas the contemporaneous plattenkalks more to the east belong to the Painten Formation. The geologically younger Mörnsheim Formation lies on top of both these formations. Biostratigraphic dating,

namely based on ammonite assemblages, shows that the base of the Altmühltal Formation begins with the latest Kimmeridgian (uppermost horizon of the *Beckeri* zone) and ends with the early Tithonian *rueppelianus* horizon of the *Hybonotum* zone, crossing five ammonite horizons. Within the Altmühltal Formation around Solnhofen and Eichstätt, the lithographic limestones of the Eichstätt Member are somewhat older than the Solnhofen Member (Schweigert 2007; Niebuhr and Pürner 2014; Schweigert 2015). In more eastern areas, the upper part of the Torleite Formation, which underlies the Painten Formation, yielded important vertebrate fossils as well. Due to this geographic, geologic and stratigraphic complexity, the "Solnhofen assemblage" should be more appropriately referred to as the "fossil assemblage of the Late Jurassic Solnhofen Archipelago" (cf. "fauna of the Solnhofen Archipelago" of Röper (2005), López-Arbarello and Schröder (2014) and Rauhut et al. (2017, 2019)). The reason for replacing "fauna" with "assemblage" is that the sediment barely preserves a single event taphocoenosis, which would represent at least the sampling of a fauna *sensu* extant biology. The term "Late Jurassic" was added here, because Solnhofen is a recent geographic marker.

The Mörnsheim Formation has its most productive outcrops in the quarries between Mörnsheim, Solnhofen (Fig. 1), Monheim and Daiting. Lithologically, the Mörnsheim Formation differs from the Altmühltal Formation in having a considerably higher number of silicified limestone beds ("Kieselplattenkalke"), especially in its lower part (Fig. 2). Biostratigraphically, this unit represents the topmost horizon of the *Hybonotum* zone, the *moernsheimensis* horizon and is, thus, slightly younger than the upper Solnhofen Member of the Altmühltal Formation. Fossils have long been known from the Mörnsheim Formation, mainly from the quarries around Daiting (Tischlinger 2001). However, the study of the faunal assemblage from the sediments of this formation is still in its infancy, because this unit has never been quarried extensively for commercial purposes due to the very limited economic utility of these rocks.

The Mörnsheim Formation at the Schaudiberg quarry is highly fossiliferous. The assemblage is dominated by strongly compacted ammonites and preserves a diversity of other invertebrates and vertebrates. In contrast to the underlying Altmühltal Formation, most vertebrate fossils in the Mörnsheim Formation are at least partially disarticulated and often fragmentary, suggesting a different taphonomic context. In the Schaudiberg quarries, gnathostome "fishes" are represented by chondrichthyans, including well-preserved specimens of *Asteracanthus* (Pfeil 2011), actinopterygians (for example, Schröder and López-Arbarello (2013)) and mainly isolated remains of coelacanths. Tetrapods are represented by hitherto unstudied turtles, rhynchocephalians, thalattosuchian and atoposaurid crocodyliforms, an avialan theropod and pterosaurs (Heyng et al. 2011; Moser and Rauhut 2011; Rauhut et al. 2011; Rauhut et al. 2012; Rauhut 2012; Heyng et al. 2015; Rauhut et al. 2019; Hone et al. 2023). The only tetrapod taxa described so far from the Mühlheim area are the unusual rhynchocephalian *Oenosaurus muehlheimensis* Rauhut et al., 2012, the pterosaur *Petrodactyle wellnhoferi* Hone et al., 2023 and the avialan theropod *Alcmonavis poescheli* Rauhut et al., 2019. The only other theropod specimen from the Mörnsheim Formation is the fragmentary holotype of *Archaeopteryx albersdoerferi*, which comes from the quarry area around Daiting (Tischlinger 2009; Kundrát et al. 2019).

Like *Alcmonavis poeschli*, the new Urvogel specimen described herein comes from the Schaudiberg quarry, near Mühlheim, in the vicinity of the market village of Mörnsheim (Fig. 1). There are two active quarries in close vicinity, both of which belong to the "Grundstücksgemeinschaft Pöschl/Leonhardt". One of the quarries, the "Fossilien-Besucher-Steinbruch" (translated as "visitors' fossil quarry") is mainly attended by private fossil collectors and hobby palaeontologists, whereas the Old Schöpfel Quarry is systematically being excavated for fossils (see Heyng et al. (2015)). The lower part of the Mörnsheim Formation has a total thickness of approximately 50 m at the Schaudiberg. To date, only parts of these layers are exposed in both of these quarries. Some 8 m of the lowermost Mörnsheim Formation outcrop in the Old Schöpfel Quarry, with the boundary to the underlying Altmühltal Formation at the base of the section, is currently covered by debris. Thus, the currently exposed section starts some 4 m above this boundary with silicified laminated limestones and intercalated thick layers of massive limestones and silicified limestones (Heyng et al. 2015: Fig. 2). In the higher part of the profile and the visitors' quarry, the section becomes more dominated by laminated limestones and intercalations of laminated marly limestones and clays (Fig. 2).

Discovery

The specimen (SMNK-PAL 10,000a) was discovered by one of us (JJWW) on Friday the 31 May 2019 in the lowest exposed layer of the "Fossilien-Besuchersteinbruch Mühlheim" at Mörnsheim (district Eichstätt, which is about 85 km south of Nuremberg), Bavaria, south Germany (48°51'18.01"N, 10°59'13.99"E), within undescribed layers, 2.5 m below the marker layer called "Dicke Emma" ("Fat Emma") from the Early Cretaceous and 1.5 m below the Late Jurassic "Vierte Rosa" ("4th Pink", Fig. 2). The exact stratigraphy of the Late Jurassic layers below the "Vierte Rosa", which defines the current bottom of the quarry, is not well understood and requires a more detailed examination. Due to the brittle and clayey nature of its layer, the specimen broke into nine pieces (Figs 3A, B, 10, 11). Those three that contain the right forelimb (Fig. 4) were carefully removed from the brittle surrounding matrix (Fig. 3B). Due to the cautious and professional removal, it was possible to reorganise these pieces and to prepare the preserved forelimb bones. Two further pieces that were found next to the specimen

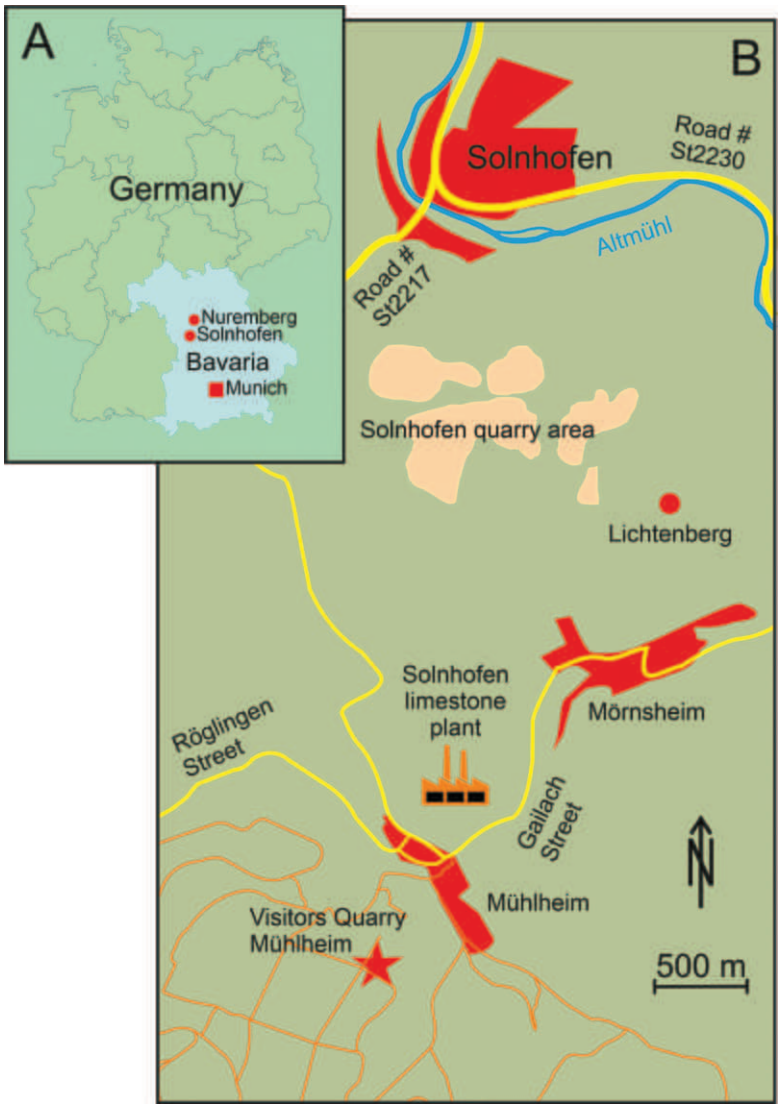

Figure 1. Geography of the discovery area. **A.** Map of Germany; Bavaria is in blue with the relevant cities marked; **B.** Map of the Solnhofen area; the quarry of discovery is located in a very remote area to the south of Solnhofen.

comprise a fragment of long bone, which could be the remains of the left humeral shaft distal to the deltopectoral crest and the middle segments of the radius and ulna from the left forelimb (SMNK-PAL 10,000b; Figs 5B, B', 9) lying near their anatomical position, suggesting that the specimen may originally have been much more complete. Later, three more pieces were unearthed, containing remains of the left and right hind limb (SMNK-PAL 10,000c; Figs. 5C, C', D, D', 10, 11). Although the area was intensively searched after the discovery, no further elements of the specimen were found.

Materials and methods

Institutional Abbreviations

BMNH: Beijing Natural History Museum (Beijing, China); **HGM**: Henan Geological Museum (Henan, China); **IVPP**: Institute of Vertebrate Palaeontology and Palaeoanthropology (Beijing, China); **JZT**: Jizantang Palaeontological Museum (Liaoning, China); **KIT**: Karlsruhe Institute of Technology (Karlsruhe, Germany); **MPCA**: Museo Provincial Carlos Ameghino (Cipolletti, Argentina); **PKUP**: Institute of Prehistoric Life and Environment, Geology Department, Peking University (Beijing, China); **SMNK**: Staatliches Museum für Naturkunde Karlsruhe (Karlsruhe, Germany); **STM**: Shandong Tianyu Museum of Nature (Pingyi, China); **TM**: Teylers Museum, (Haarlem, Netherlands); **YFGP**: Yizhou Fossil and Geology Park (Liaoning, China)

Standard photography

Photos under natural light were taken with a Lumix G9 with a Lumix 12–60 mm F3.5-5.6 OIS lens for overviews and an Olympus M. Zuiko Digital ED 60 mm f/2.8 Macro for details. For macro photography, a Godox TT685IIF external flash gun was used in TTL mode.

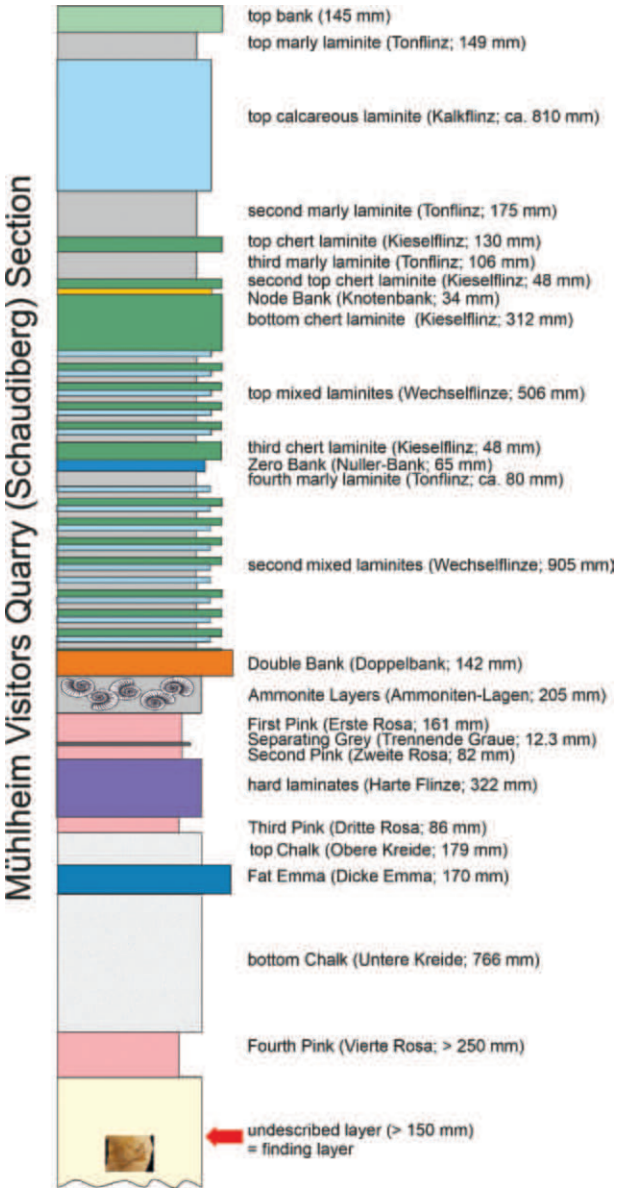

Figure 2. Geological section of the Mühlheim "Visitor`s Fossil Quarry" outcrop at Schaudiberg (modified after Heygn (2015)).

Ultraviolet (UV) photography

For UV documentation, three high-intensity Benda UV hand lamps (type N, 16 W) and a wavelength of 365–366 nm (UV-A) were used. The hand lamps contained two 8 W UV tubes, which provided an even illumination of the specimen. For some images, a high-performance Labino UV-A lamp (Spotlight S 135, 35 W, 365 nm) equipped with a custom-made mid-light-reflector inset was also used. Photos were taken with a Lumix GX80 with a Lumix G 30 mm f/2.8 Macro OIS lens.

X-ray computed tomography (CT)

X-ray CT scans of the individual slabs were performed at the Laboratory for X-ray Computed Laminography and Tomography of the IPS at KIT. A micro-focus X-ray tube (XWT-225, X-RAY WorX, Garbsen, Germany) was employed and operated at an acceleration voltage of 200 kV and a target power of 25 W. The spectrum was externally filtered with 2 mm copper to suppress beam hardening effects. The slabs were placed 182 mm and the X-ray detector was placed 1,710 mm away from the X-ray tube, resulting in a geometrical magnification of 9.4. For X-ray detection, a flat-panel detector with a physical pixel size of 200 µm (XRD 1621 CN14 ES, PerkinElmer, Waltham, USA) was used, thus resulting in an effective pixel size of 21.24 µm. For each tomogram, 2,048 projections were acquired that were equally distributed over a full 360° rotation of the sample, each exposed for 24 s. The main slab was scanned in four steps to cover the full fossil. Tomographic reconstructions were performed by using the in-house developed UFO framework with tofu (Faragó et al. 2022).

Post-processing of tomographic data

For further processing, the tomographic datasets were converted to 8-bit, cropped to the regions of interest and imported into Amira 5.6. The four single volumes of the main slab were registered and merged. The bones in all slabs were pre-segmented in the software's segmentation editor. Automatic interpolation between the pre-segmented slices was done using the online platform Biomedisa (https://biomedisa.info) (Lösel et al. 2020). The results were re-imported into Amira and minor errors corrected. The final segmentation results were converted into polygon meshes, exported as OBJ files and then re-assembled, smoothed and rendered with CINEMA 4D R20 (https://www.maxon.net/de/cinema-4d).

Geometric morphometrics (GMM) of manual unguals

To aid in the taxonomic diagnosis of the isolated manual ungual, GMM analysis was conducted via principal component analysis (PCA) and canonical discriminant analysis (CDA) (Zelditch et al. 2012). A total of 48 manual unguals were analysed, comprising 27 from 12 Urvogel specimens and 21 from 11 specimens of *Anchiornis* (see Suppl. material 1). The Urvögel comprised nine specimens unequivocally identified as *Archaeopteryx* (22 unguals), along with SMNK-PAL 10,000a (1), the Mühlheim specimen (*Alcmonavis*; 3) and the Haarlem specimen (*Ostromia*; 1). *Anchiornis* was chosen given the recovery of the Haarlem specimen as *Ostromia* within Anchiornithinae by Foth and Rauhut (2017), as well as the phylogenetic proximity to *Archaeopteryx*. An image of the CT scan data of SMNK-PAL 10,000a was used in place of an *in-situ* photo for landmarking to avoid occlusion by the matrix or confounding from the camera angle. The manual unguals of the Berlin specimen of *Archaeopteryx* are not coplanar with the matrix; as such,

available photographs of these unguals are skewed. To correct for this, a 3D photogrammetric reconstruction of the unguals was performed with RealityCapture 1.4 (Capturing Reality). The generated models were exported to Meshmixer 3.5.474 (Autodesk) and aligned so that images perpendicular to each ungual plane could be taken and used for more accurate landmarking. Landmarks were placed at the proximal base of the dorsal curvature, excluding the ungual lip (as it is damaged in SMNK-PAL 10,000a); the tip of the claw; and the apex of the flexor tubercle. Semi-landmarks were equally placed along dorsal and ventral curvatures, each numbering 28 for the PCA (to capture the ungual shape with high resolution) as well as seven and three for the CDA (which are limited by sample size). No landmarks or semi-landmarks were placed along the articular surface or the proximal flexor tubercle, as they are damaged in SMNK-PAL 10,000a.

All GMM analyses were conducted in R (RStudio Team 2020; R Core Team 2021). The digitisation of landmarks and semi-landmarks was performed using the R package StereoMorph (Olsen and Westneat 2015). General Procrustes analysis (GPA) was used to align and scale the landmarks. The procD.lm function was used to test for an allometric signal (correlation between the landmark coordinates and the centroid size). PCA was used to identify and visualise the primary axes of variation in morphology. In addition to these analyses, thin-plate splines were generated to visually represent shape changes. The thin-plate spline generation, GPA, allometry test and PCA were each performed using the R package geomorph (Adams et al. 2023). CDA was performed using the R package MorphoTools2 (Šlenker et al. 2022). Plots were created and edited using R package ggplot2 along with cowplot, ggrepel, Magick and svglite (Wickham 2016; Wickham et al. 2023; Wilke 2024; Slowikowski 2024; Ooms 2024).

CDA explores morphological variation of two or more groups by minimising intra-group variance and maximising inter-group variance, for evaluating if the groups can actually be separated from each other. CDA was used to compare the ungual morphology of SMNK-PAL 10.000 with that of *Archaeopteryx*, *Anchiornis*, the Haarlem (*Ostromia*) and the Mühlheim (*Alcmonavis*) specimens. The sample of known *Archaeopteryx* and *Anchiornis* acted as the training dataset, while SMNK-PAL 10,000, the Haarlem and Mühlheim specimens were included passively as 'mystery specimen' (meaning that they do not provide information for the CDA), given the small sample size for the two latter specimens and that their taxonomic validity is disputed amongst the authors.

PCA and CDA were also used to compare the morphologies of only ungual II, the presumed identity of the manual ungual in the new specimen (see below). This provided a more direct comparison, as the morphological variation between unguals I, II and III in *Archaeopteryx* may be distinct from that seen in *Anchiornis* and, thereby, act as a confounding variable. This, in turn, helped to account for the possibility that an *Archaeopteryx* ungual II might be distinct from an *Anchiornis* ungual II, but similar to an *Anchiornis* ungual III. As the removal of unguals I and III from this analysis reduced the total number of specimens, the CDA must be restricted to nine total landmarks (including three semi-landmarks each for the dorsal and ventral curvatures).

Phylogenetic analysis

To determine the phylogenetic position of the new specimen, we used a revised version of the matrix of Rauhut et al. (2019), which encodes for the interrelationships of Coelurosauria. Several character definitions were modified, a few characters were deleted, others were added and numerous scorings were checked and modified (see Suppl. material 2). The genera *Hagryphus* and *Eosinopteryx* were deleted from the current matrix because their scorings need a careful revision. Furthermore, the taxonomic status of *Eosinopteryx* is questionable. According to Pei et al. (2017), *Eosinopteryx* is more or less similar to *Anchiornis*, except for the tail length, which is much shorter in the former species. However, Hu et al. (2018) suggested that the tail of the specimen is incomplete and a severe breakage between the 10th and 11th caudal vertebrae may indicate that the short tail could result from a potential manipulation during preparation (see Rowe et al. (2001); Stone (2010); Balter (2013); Agnolín et al. (2019)). However, this needs to be evaluated by first-hand examination of the specimen. In contrast, we added the following genera to the dataset: *Ceratosaurus* (new outgroup taxon), *Alioramus*, *Ambopteryx*, *Aniksosaurus*, *Aorun*, *Appalachiosaurus*, *Archaeorhynchus*, *Aristosuchus*, *Bagaraatan*, *Bannykus*, *Bicentenaria*, *Bistahieversor*, *Caihong*, *Dakotaraptor*, *Daliansaurus*, *Dineobellator*, *Dromaius*, *Dryptosaurus*, *Epichirostenotes*, *Fukuivenator*, *Gobivenator*, *Jianchangosaurus*, *Juratyrant*, *Kileskus*, *Liaoningvenator*, *Linheraptor*, *Lythronax*, *Mirischia*, *Nqwebasaurus*, *Oksoko*, *Qianzhousaurus*, *Serikornis*, *Shishugounykus*, *Shri*, *Sinocalliopteryx*, *Suskityrannus*, *Teratophoneus*, *Tugulusaurus*, *Xinjiangovenator*, *Xiyunykus*, *Xunmenglong*, *Yi* and *Zuolong*.

Furthermore, the genus *Compsognathus* was split into its two original species, *C. longipes* and *C. corallestris*, following Ostrom (1978; pers. obs. OWMR).

Characters and character states that refer to furrows along the main axis of the radius, metacarpals and phalanges were deleted, as a taphonomic artefact cannot be ruled out for those taxa that suffered impaction through compression during the fossilisation process (see Discussion).

The final matrix comprises 179 terminal taxa, was coded for 597 characters (Suppl. materials 3, 4) and was analysed with the software *TNT*, version 1.6 (Goloboff and Morales 2023; Fig. 13), using the New Technology search (with all four search methods – sect. search,

ratchet, drift and tree fusing – with a driven search to find the minimal length 100 times), followed by TBR branch swapping. The matrix was analysed with equally weighted and implied weighted (k = 12) characters (Goloboff et al. 2018). To evaluate node support, 1,000 bootstrap replicates were calculated. The consistency index (CI) and retention index (RI) of the most parsimonious trees, as well as the tree lengths of alternative topologies, were estimated in *Mesquite* 3.7 (Maddison and Maddison 2021). Afterwards, the most parsimonious trees obtained were summarised using strict consensus and reduced strict consensus methods (Wilkinson 1994; Pol and Escapa 2009), with *Albinykus*, *Aristosuchus*, *Bicentenaria*, *Hesperonychus*, *Liaoningvenator*, *Lythronax*, *Oksoko*, *Pelecanimimus*, *Songlingornis* and *Xinjiangvenator* being pruned from the set of trees for the equally weighted character dataset and *Aristosuchus*, *Byronosaurus*, *Dakotaraptor*, *Hesperonychus*, IGM100/44, *Pyroraptor* and *Xinjiangvenator* being pruned from the set of trees for the implied weighted characters.

Preservation

The specimen as found consists of nine limestone slabs (Figs 3–5, 10, 11), the surfaces of which are brittle and flaky. The bones show numerous compaction and impaction cracks. In places, the compacta has flaked off, especially on the anteromedial face of the left coracoid and the deltopectoral crest of the humerus (Figs 4, 5). Small parts of bones are missing, others are preserved as external moulds.

The composed main slab (Figs 3B, 5A, A', 4, 6) comprises an almost articulated right forelimb, which lacks most elements of the manus, namely the digits. Of the scapula, only the area of the collum, including the anterior half of the roof of the glenoid fossa is preserved. The fragment has rotated anteriorly and, thus, has slightly separated from the coracoid. Both bones are seen in medial aspect. Of the furcula, only the left and right rami are preserved (Figs 5A, A', 6, 7). The missing middle part is preserved as an external mould (filled with glue) allowing for a reliable reconstruction of the morphology of the bone (Figs 7, 12). The extremity of the right ramus of the furcula articulates with the scapulocoracoid complex exactly at the articulation of the two bones. The humerus is seen in posterolateral aspect (Figs 4, 6). The bone has rotated posteriorly and shifted posterolaterally. The margin of its caput now lies along the dorsal half of the lateral margin of the coracoid.

The radius and ulna have rotated posteriorly and are orientated perpendicularly to the humeral shaft (Figs 4, 5A, A', 6, 8). The ulna is seen in medial aspect, still in articulation with the dorsal condyle. The radius has disarticulated, with its caput shifted a few millimetres proximally. It exposes its anterior face. Distally, both bones lie in contact with each other (Fig. 8).

The carpals are missing, with the probable exception of one. The tiny bone lies close to the anterior face of the distal articular head of the radius. It likely represents the right radial carpal (Figs 3A, 4–6, 8). Nevertheless, the region between the ulna/radius and the metacarpals suffered from a huge break, the fragments of which have been reconstructed as well as possible. Thus, it cannot be ruled out that other carpal bones were originally present.

Only the proximal two-thirds of metacarpals II and III are preserved. They are seen in dorsal aspect, parallel to each other and in close contact, but are disarticulated from the carpus. Metacarpal II is partially overlain by the distal articular end of the ulna. The angle between the metacarpus and ulna/radius is about 120° (Figs 4, 5A, A', 6, 8).

Of the basal phalanx of digit I, the proximal two-thirds are preserved. The bone lies at an angle of 5° against metacarpal III and overlies the distal third of the latter. The penultimate phalanx of digit II is isolated and lies at an angle of 2° to the shaft of the radius. The proximal articulation almost contacts the dorsal face of the radius. The ungual phalanx of the same digit is isolated as well and lies adjacent to the anterior margin of the distal sixth of the humerus. The articular area of the ungual is missing, as is the proximal-most part of the flexor tubercle (Fig. 8).

One of the other two slabs comprises the shafts of the left radius and ulna, which are preserved in a near natural configuration (Fig. 9A). All articular ends are missing or incomplete. The second slab bears a fragment that may represent the remains of the left humeral shaft distal to the deltopectoral process (Fig. 9B). However, due to its fragmentary nature, this identification has to be taken with caution. The preservation style of the bone is coincident with that of the main slab.

The hind limb fragments (Figs 5C, C', D, D', 10, 11) are preserved on three slabs. The elements of the left hind limb are preserved on one slab. With the exception of the middle fourth of the femoral shaft, where the compacta shows a similar compaction pattern to that of the right limb elements, the bones are pulverised (Figs 5D, D', 10). Both articular ends of the femur are missing, as are the proximal articular ends of the crural bones. Still, it is evident that the left femur and crural bones are preserved in articulation. The individual crural bones cannot be identified due to massive crushing (Figs 5D, D', 10).

The right femur and the proximal ends of the right tibia and fibula are preserved across two slabs (Fig. 11). The compacta of the right hind limb elements show compaction fractures. The right femur is likely seen in posterior aspect, based on its curvature and the location of the intercondylar sulcus (Fig. 11). Both the proximal and distal articular heads of the right femur are missing. The tibial fragment is seen in posterior aspect, with both articular condyli being exposed (Figs 10, 11). Most of the fibular head is preserved as an external mould. The rest of the fragment is preserved in a way that nothing can be said about the orientation of the bone.

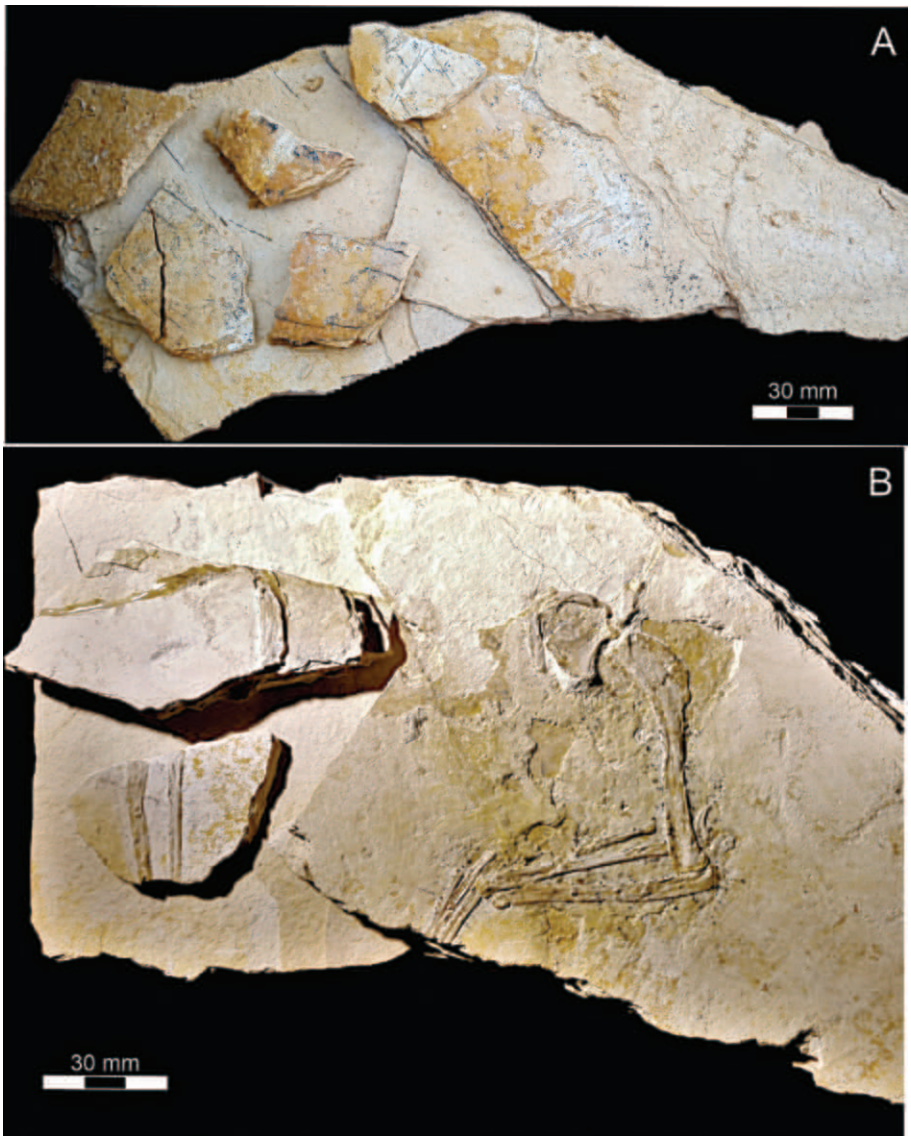

Figure 3. SMNK-PAL 10,000a-b. **A.** Original condition of the slabs prior to preparation; **B.** Slabs containing remains of the left arm and fragments of the right one after the first preparation.

Systematic palaeontology

Theropoda Marsh, 1881
Maniraptora Gauthier, 1986
Avialae Gauthier, 1986

cf. *Archaeopteryx* sp.

Note. The specimen is housed in the palaeontology collection of the State Museum of Natural History Karlsruhe (SMNK) under the registration numbers SMNK-PAL 10,000a-c. Following the historical naming convention of Urvögel, based on repository, we propose to informally refer to this fossil as the "Karlsruhe specimen".

Locality. Schaudiberg, near Mühlheim, at Mörnsheim (DistrictEichstätt),Bavaria,southGermany(48°51'18.01"N, 10°59'13.99"E; Fig. 1), "Fossilien-Besucher-Steinbruch", at that time Grundstücksgemeinschaft (common property) Pöschl/Leonhardt.

Horizon. Mörnsheim Formation, lower Tithonian, undescribed layer, 1.5 m below the marker layer "Vierte Rosa" ("Fourth pink"; Fig. 2).

Description. ***Comments on the orientation of elements*.** Because the forelimb and the pectoral girdle in particular have undergone considerable changes in orientation during the evolution from early reptiles to birds, a clarification of how we orientate these elements for the description seems necessary. Whereas the scapula is positioned almost vertically with respect to the vertebral column in basal amniotes (see Schwarz et al. (2007)), it is more or less parallel to the vertebral column in birds and derived non-avian paravians (for example, Pei et al. (2017)), including *Archaeopteryx* (Wellnhofer 2009). Thus, the originally anterior side of the scapula becomes the dorsal side, the posterior side the ventral side and so on. We use the bird-like orientation for the description of the scapula, because this seems to be much closer to the real orientation in *Archaeopteryx* than the original

Figure 4. SMNK-PAL 10,000a. Main slab containing the right arm under normal light; note the brittle consistency of the surface of the slab.

reptile-like orientation of this bone. As for the coracoid, the matter is even more complicated. In modern reptiles, the coracoids are more or less aligned with the scapulae and approach the body mid-line below the latter element. Thus, they have an anterior, posterior, medioventral and laterodorsal edge. In birds, the coracoid is strongly angled towards the scapula (often in a sharp angle of less than 90°) and the ventral end is twisted against the dorsal end, so that the originally posterior side becomes the lateral side ventrally. This re-orientation and twist of the coracoid seems to have happened gradually during the evolution of birds (see Ostrom (1976); Mayr (2017)). Whereas Ostrom (1976: Fig. 4B) and Carney (2016: fig. II.8) reconstructed *Archaeopteryx* with an angle of approximately 90° between this bone and the scapula and an almost entirely lateromedially orientated ventral end of the coracoid, Mayr (2017: fig. 1a) illustrated the coracoid of this taxon still more aligned with the scapula, at an angle of much more than 90° and with an anterodorsomedially-posteroventrolaterally orientated distal end. In other basal paravian theropods, in which the shoulder girdle is known in 3D preservation, the situation varies. In many taxa, such as *Velociraptor* (Norell and Makovicky 1999), *Adasaurus* (Perle et al. 1999), *Sinovenator* (Xu et al. 2002), *Mei* (IVPP V12733; Xu and Norell (2004)) and *Sinornithoides* (Russell and Dong 1993), the coracoid is largely aligned with the scapula, being only markedly flexed medially and slightly angled ventrally. An exception is *Buitreraptor*, in which the coracoid is more elongate than in other paravians, has a constricted neck, a marked angle towards the scapula and a notable twist (MPCA 245; Gianechini et al. (2018)); thus, much more resembling the condition in birds, with the ventral end showing a largely mediolateral orientation. However, this is the exception in non-avian paravians and phylogenetic analysis indicates that this condition was acquired convergently to birds in *Buitreraptor*. Herein, the *Archaeopteryx* coracoid is considered to have a mediodorsal margin, a laterodorsal margin that articulates with the scapula, a lateroventral margin and a medioventral margin that articulated with the (still unknown) sternum.

As for the bones of the forelimb, the re-orientation of the pectoral girdle and the limb also has consequences for the orientation of these elements. Thus, in non-avian dinosaurs with an erect limb posture, usually a proximal and distal end and anterior, medial, posterior and lateral sides are distinguished, whereas the laterally-held stylopod and zeugopod of birds have an anterior, dorsal, posterior and ventral side. Here we adhere to the orientational terms for non-avian dinosaurs, also to avoid confusion with the orientation of the humerus in other reptiles (for example, lepidosaurs), in which the dorsal side of this bone corresponds to the posterior side in non-avian dinosaurs and not to the lateral side (as is the case for the dorsal side of the humerus in birds).

Furcula (Figs 4, 5A, A', 6, 7, 12A, A'). The furcula is seen in anterior aspect. Despite missing the middle part of the U-shaped bone, the tip of the ventral ramus, the ventral margin of the right ramus and fragments of the right terminus, the external mould allows for a precise reconstruction. The furcula is oval in cross-section, with its height about twice its depth. The aperture angle of the U is about 80°. The slight difference of the aperture angle with other *Archaeopteryx* specimens (London, Daiting and Thermopolis) is likely due to compaction. The right terminus of the furcula lies in articulation with the acromial region of the scapula as revealed by the digital reconstruction.

Scapula (Figs 5A, 6, 7, 12A, A'). Of the right scapula, only the collum and the anterior half of the glenoid facet is preserved, exposing its medial face. The scapula has rotated anterodorsally against the coracoid at an angle of about 15° in a way that the facies articularis coracoidei is now facing the facies articularis humeralis coracoidei. Of the scapular blade, only a partial external mould of the ventral margin is visible. As in other specimens of *Archaeopteryx* (for example, Mayr et al. (2007); Tischlinger (2009); Rauhut et al. (2018)), a dorsally expanded acromial process is absent and the dorsal margin of the supraglenoidal region is continuous with the dorsal margin of the shaft. Instead, an anteriorly directed acromial process is present, a remnant of which is preserved below the coracoid, as is seen in the tomography scans (Figs 5A', 12A, A'). These scans also reveal that the base of this process bulged slightly laterally, as is also the case in the Thermopolis specimen (Mayr et al. 2007). The medial face dorsal to the dorsal lip of the facies articularis humeralis is concave and shows a slightly thickened medial margin. This part likely represents a constriction at the ventral base of the acromial region that separated the process from the facies articularis coracoidalis. Ventral to this concavity, the anterior margin of the facies articularis coracoidalis becomes evenly convex, forming an elongate ovoid articular face, which is set off from the medial face of the corpus by a low ridge and probably corresponds to the tuberculum coracoideum of modern birds.

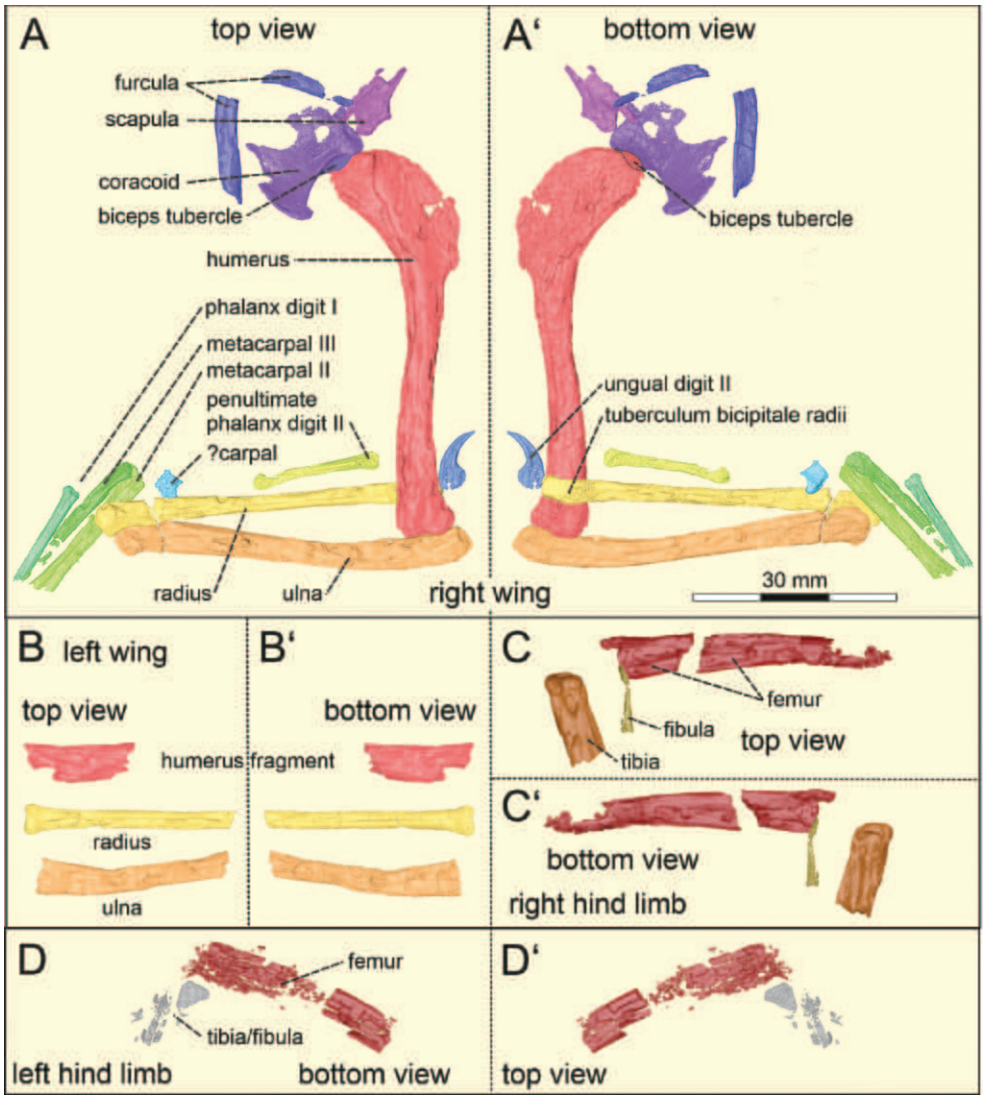

Figure 5. SMNK-PAL 10,000a-c, digital 3D reconstructions based on tomography of all parts of the specimen. **A.** Exposed top and **A'.** Embedded (in matrix) bottom views of the right arm and shoulder in SMNK-PAL 10,000a; note the presence of a tuberculum bicipitale radii; **B.** Exposed top and **B'.** Embedded bottom view of the left arm consisting of fragments including the left radius and ulna of SMNK-PAL 10,000b; **C.** Exposed top and **C'.** Embedded bottom views of the left hind limb of SMNK-PAL 10,000c; **D.** Exposed top and **D'.** Embedded bottom views of the right hind limb of SMNK-PAL 10,000c.

With the exception of the above-mentioned concavity, the facies articularis coracoidalis is missing. The dorsal third of the scapular corpus is damaged. The facies articularis humeralis is separated from the facies articularis coracoidalis by a strongly convex bulge and stands at an angle of about 160° to the facies articularis coracoidalis. The articular surface of the facies articularis humeralis scapulae is characterised by a shallow oval depression surrounded by a blunt wall on the medial side. As in most paravian theropods and other specimens of *Archaeopteryx* (for example, Tischlinger (2009); Carney (2016)), the actual articular surface was on the lateral side of the bone and faced lateroventrally.

Coracoid (Figs 4, 5A, A', 6, 7, 12). The coracoid is seen in internal aspect. The facies articularis scapulae and the surrounding compacta of the foramen coracoideum are damaged. The compacta of the mediodorsal third of the medial face of the bone is also missing. Most of the mediodorsal half of the facies articularis sternalis is preserved as an external mould. Despite the damage, the shape of the coracoid can be reliably reconstructed.

The bone is hatchet-shaped, with its dorsal margin being two-thirds the length of the facies articularis sternalis. The facies articularis scapularis at the laterodorsal margin of the bone is broken, but appears to have been confluent with medial side of the facies articularis humeralis coracoidei, which has the same length as its scapular counterpart as preserved. The surface of the facies articularis humeralis coracoidei is slightly concave transversely and slightly expanded by a medial lip. The width of this lip increases towards the lateral margin of the coracoid. The outline of the articular face itself is difficult to assess,

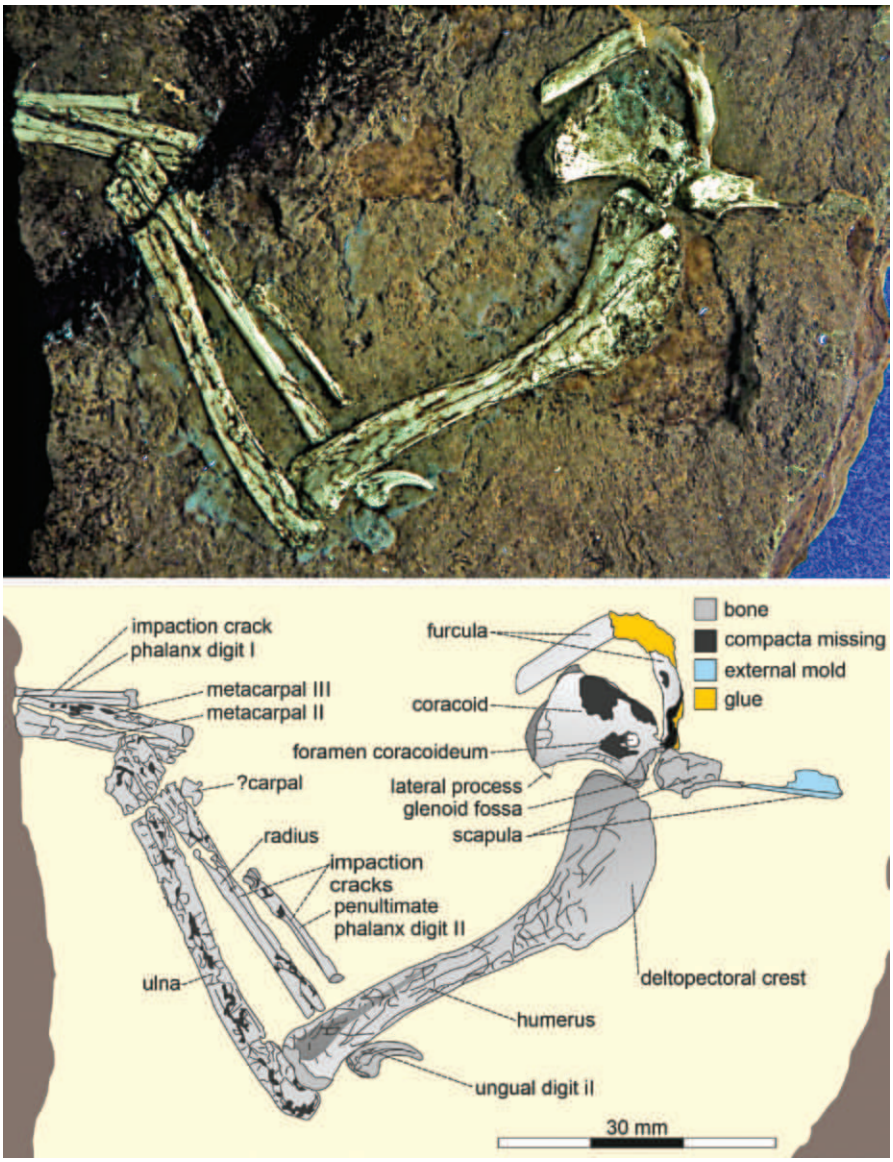

Figure 6. SMNK-PAL 10,000a, right forelimb prior to preparation. Top: under filtered UV-light; bottom: interpretive drawing.

especially as it is exposed in medial aspect. As in other paravian theropods, most of the articular facet probably faced laterally. It appears to have been a rounded trapezoid in outline, with its ventral margin being one-third wider than its dorsal one. The dorsal three-fourths of the articular face are slightly transversely concave.

As is concluded from the remnants, the mediodorsal margin of the bone must have been evenly convex, curving into the evenly convex sternal (medioventral) margin. The lateral margin of the coracoid is concave. Near its ventral termination, the margin abruptly continues into a blunt and short process ("sternal process" of Norell and Makovicky (1999); corresponds to the lateral process of modern birds; see also Mayr et al. (2007)), which also forms the lateral continuation of the facies articularis sternalis. A similarly offset sternal process is also present in *Archaeopteryx*, *Jeholornis* and some dromaeosaurids (Ostrom 1974; Norell and Makovicky 1999; Zhou and Zhang 2002; Mayr et al. 2007). A blunt ridge is present along the posterior side of the lateroventral margin of the coracoid. It is slender and tapers towards the sternal process. The facies articularis sternalis is convex with an increasing curvature in its lateroventral third.

The medioventrally-laterodorsally orientated, oval foramen supracoracoideum pierces the centre of the laterodorsal fourth of the coracoid. Despite the flaked-off ventral margin and surrounding compacta, its shape is clearly visible. Its width is about two-thirds its height.

The tomographic scans reveal a prominent disc-like structure between the coracoid and humeral head, which is still embedded in the matrix. The structure is placed in the dorsal third of the lateral margin and emerges from the anterior surface of the coracoid right next to the lateral margin. The structure is dorsoventrally elongated and bears a convex margin, the tip of which protrudes beyond the humeral head (Fig. 12 A, A'). However, its lateral position is probably due to compaction, while *in vivo* the structure would probably be facing more anterolaterally.

Based on its positions, the structure could correspond to the biceps tubercle (coracoid tubercle), resembling that of *Archaeopteryx* in shape and size (Mayr et al. 2007; Carney 2016: fig. II.8).

Humerus (Figs 4, 5A, A', 6, 9B–B''). The right humerus is almost complete, but massively compacted and is seen in posterolateral aspect. It has a maximum length of 57.8 mm (Table 1), which is most similar to that of the Munich specimen (57.5 mm; Wellnhofer (2009)). In the middle of the articular facet of the humeral head, there is a shallow concavity that likely represents the contact face with the glenoid fossa. The articular facet of the humeral head is separated from the internal tuberosity by a shallow depression. The proximally rounded semi-ovoid internal tuberosity is proximodistally elongate and extends for about half the length of the humeral neck. Distally, it merges gradually with the medial margin of the shaft.

Table 1. Selected measurements from SMNK-PAL 10,000a. + = incomplete bone.

Element	Length (mm)
humerus	57.8
ulna	52.8
radius	51.3
metacarpal I	–
metacarpal II	23.4+
metacarpal III	23.7+
digit I	–
1. phalanx	16.5+
2. phalanx (ungual)	–
digit II	–
1. phalanx	–
2. phalanx	19.0
3. phalanx (ungual)	9.8+
digit III	–
1. phalanx	–
2. phalanx	–
3. phalanx	–
4. phalanx (ungual)	–

The proximal part of the humerus that houses the deltopectoral crest and the internal tuberosity is angled at about 30° against the shaft, which is almost identical to *Archaeopteryx*, but different from *Alcmonavis* (Rauhut et al. 2019). Anterolaterally, the humeral head narrows anteroposteriorly and continues into the evenly convex deltopectoral crest that extends over the proximal fourth of the humerus. At its distal end, the deltopectoral crest terminates in a low convexity that further distally sharply turns into the anterolateral margin of the shaft. The distal terminal flange is set off by a small, curved depression, which lies in continuation with the anterolateral margin of the shaft and curves towards the rim of the deltopectoral crest. It appears that this structure slightly warps into the sediment, but is mostly pressed flat. The convexity lies level with the attachment facet of m. pectoralis, which lies on the other side of the humerus in *Alcmonavis* and in modern birds (Rauhut et al. 2019; Fig. 5A'). As revealed by the scans, a true facet for the m. pectoralis is not observable on the lateral edge of the anteromedial side of the deltopectoral crest (Fig. 5A').

The anterolateral margin of the humeral shaft is slightly concave until the lateral condyle, where the concavity increases. The low bulge distal to the deltopectoral crest is due to compaction. Posteromedially, the internal tuberosity continues on to the humeral shaft with only a slight inflection of its medial margin, unlike the more offset tuberosity in the Thermopolis specimen of *Archaeopteryx*, for example (Mayr et al. 2007: fig. 10b). The posterolateral margin of the humeral shaft runs straight for about half the extent of the deltopectoral crest, then becomes concave until its mid-length. Distal to this point, the posterior margin of the humerus is slightly convex, with a short and shallow concavity proximally adjacent to the medial condyle.

The compacted distal condyles of the humerus are facing anterodistally. The lateral condyle appears regularly ball-shaped and is seen in posterolateral aspect. The medial or radial condyle has about the same size as the lateral one, with a stronger curvature, as is seen in the tomography image.

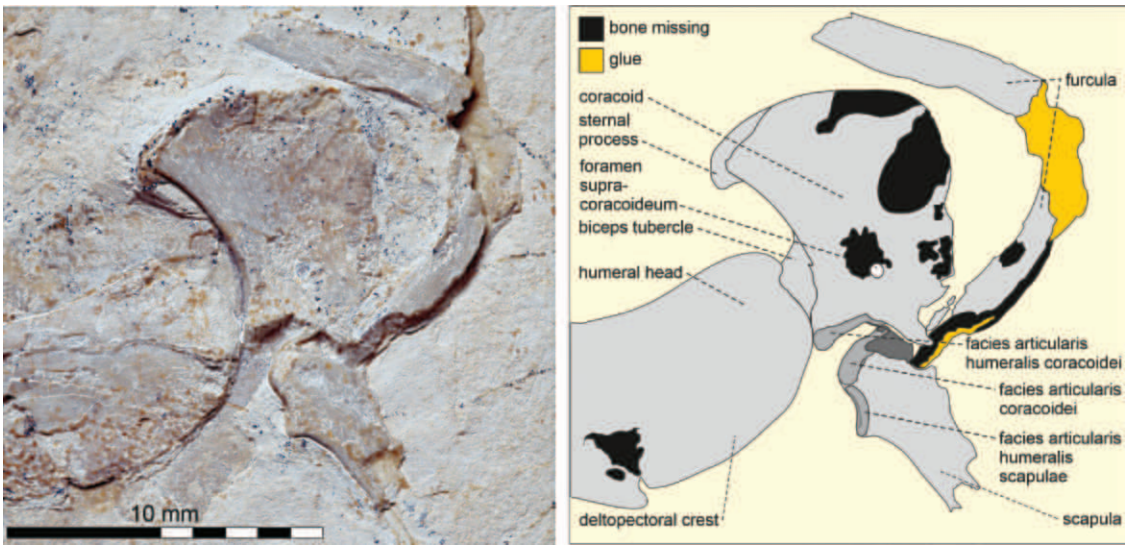

Figure 7. SMNK-PAL 10,000a, shoulder area. Left: under natural light; right: interpretive drawing.

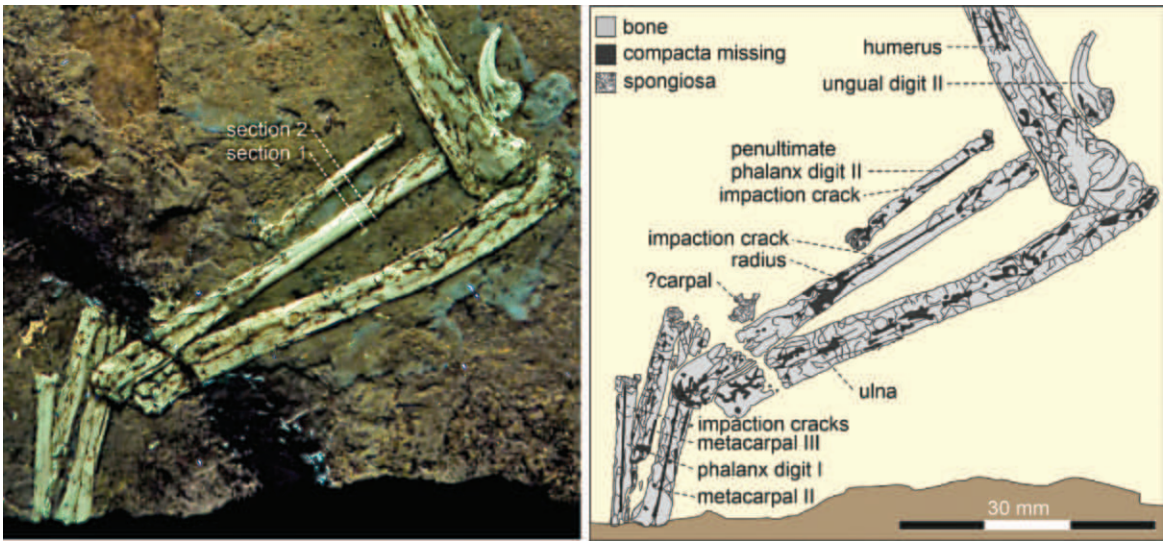

Figure 8. SMNK-PAL 10,000a, right antebrachium, carpus, metacarpus and manus. Left: under filtered UV light; section 1 corresponds to Figs. 14A and A'; section 2 corresponds to Figs. 14B and B'; right: interpretive drawing.

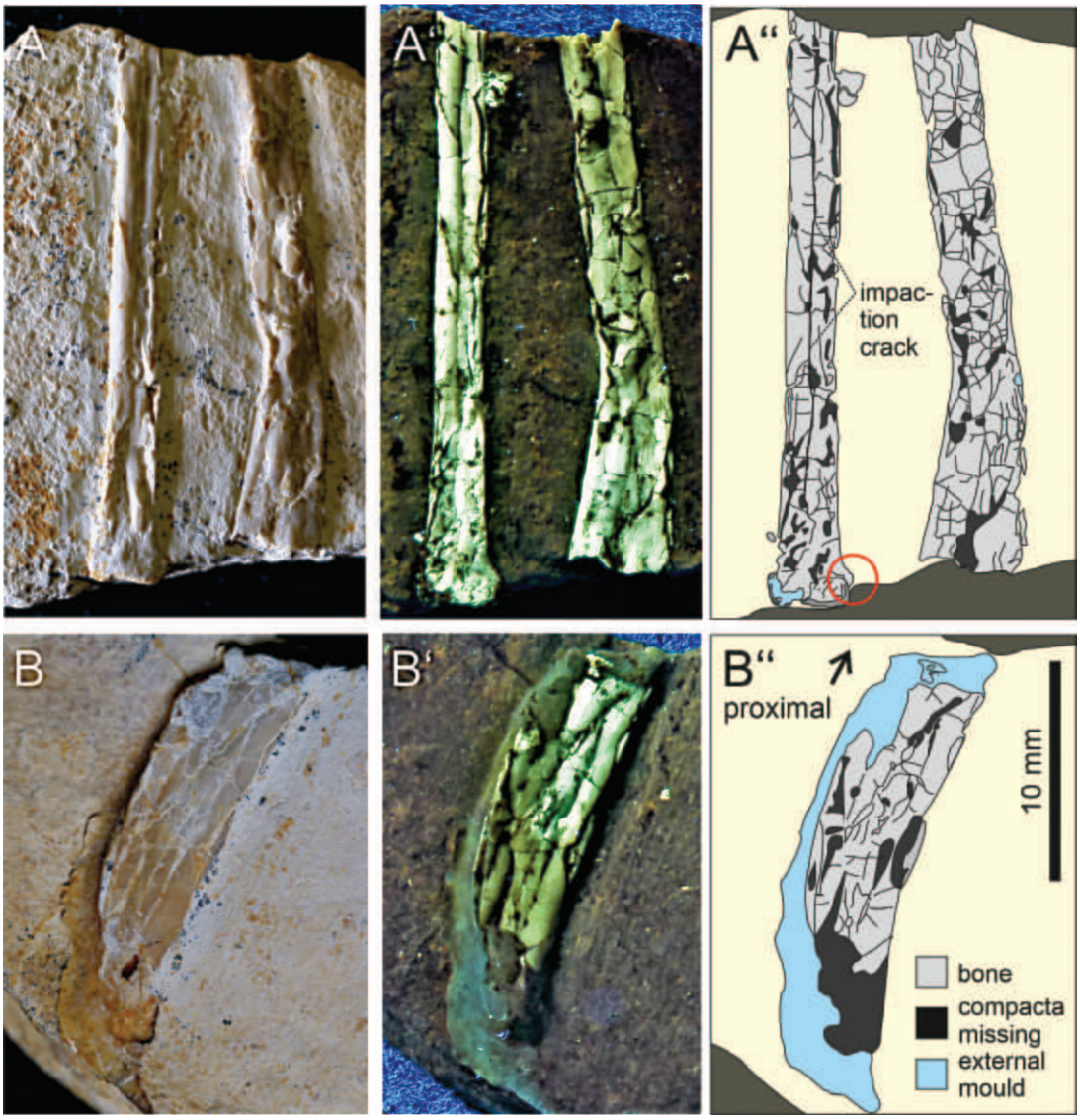

Figure 9. SMNK-PAL 10,000b, left forelimb. **A.** Radius/ulna under natural light; **A'.** Under filtered UV light; **A''.** Interpretive drawing; the circle marks the tuberculum bicipitale radii; **B.** Fragment of the left humerus under natural light; **B'.** Under filtered UV light; **B''.** Interpretive drawing.

The fragment of the left humerus (Fig. 9B-B'') comes from the mid-shaft area. Due to its massive compaction, no anatomical details are preserved.

Radius (Figs 4, 5A, A', B, B', 6, 8, 9A–A''). The proximal articular head of the right radius is overlain by the distal articular end of the humerus and is impacted (Figs 4, 5A, A', 6, 8). The bone exposes its posterior face and is 51.3 mm long. The tomography scans reveal that the proximal end bears a small, medially directed triangular process, which according to its topographical position, may represent the tuberculum bicipitale radii, similar to *Alcmonavis*, *Archaeopteryx*, *Bambiraptor*, *Confuciusornis* and *Cratonavis* (Chiappe et al. 1999; Burnham 2004; Rauhut et al. 2019; Li et al. 2023; Fig. 5A'). However, a compression artefact cannot be ruled out with certainty.

As preserved, the shaft of the radius is half as wide as that of the ulna, until the middle of the bone. From there, the lateral and medial margins diverge until the distal articular head, which is one-fourth thicker than the narrowest diameter of the shaft. The posterior face of the radius is marked by a longitudinal furrow that terminates at the proximal fifth of the bone. The distal terminus of the furrow cannot be identified due to the collapsed compacta. The cross-section shows that the furrow is evidently a result of impaction (see below, Fig. 14). The articular face of the condyle shows multiple punctures, but appears to have been markedly convex mediolaterally.

Only the shaft of the left radius is preserved (Figs 5B, 9A–A''). The proximal end of the bone expands medially, preserving the transition to the articular facet, but not the facet itself. As in the other radius, the medial expansion could indicate the presence of a tuberculum bicipitale radii. However, its morphology is hard to evaluate because the proximal end is missing. The bone is almost straight and shows a longitudinal furrow, which, at both ends, vanishes in fragmented compacta. Like on the contralateral radius, the furrow results from diagenetic impaction (see below, Fig. 14). Whether or not the longitudinal grooves that are also described for *Alcmonavis*, *Jeholornis* and various Enantiornithes (Chiappe and Walker 2002; Sanz et al. 2002; Hu et al. 2015; Rauhut et al. 2019) are similarly caused by diagenetic impaction needs to be investigated.

Ulna (Figs 4, 5A, A', B, 6, 8, 9A–A''). The right ulna (Figs 4, 5A, A', B, B', 6, 8, 9A–A'') is seen in medial aspect and is massively compressed. Its length is 52.8 mm, which is most similar to that of the Munich specimen (53.5 mm; Wellnhofer (2009)). The shaft of the ulna has a sigmoidal curvature, with the proximal half being posteriorly convex and the distal half being anteriorly convex. The proximal extremity is marked by a blunt, short and evenly rounded olecranon tubercle. The proximal terminus of which is slightly abraded, but likely had a semicircular outline in the preserved view. The proximalmost part of the shaft is parallel-sided. The trochlear notch as well as the radial tubercle are obscured by the dorsal condyle of the humerus. The narrowest point of the shaft is in its middle. The anterior third of the distal extremity – as reconstructed from the distal part of the ulnar shaft – is overlain by the distal fifth of the radius. The surface of the ulna bears four knob-like elevations that, at first glance, resemble quill knobs (but see below: Fig. 13).

The bone fragment of the left ulna is seen in medial aspect and parallels the radius fragment on the same slab (Figs 5B, B', 9A-A''). Both articular ends are missing. Distally, the ulna fragment is broken at the base of the distal curvature. Three small, circular knobs are seen, the position of which is almost identical to the three proximal ones preserved on the right ulna. Tomography evidence reveals that these knobs are crystalline, likely calcitic diagenetic artefacts. These framboid-like crystals must have precipitated prior to compaction. Similar knobs are present on the proximal end of the right humerus and the left femoral shaft, as well as on the humerus of *Alcmonavis* (Rauhut et al. 2019), indicating that this artificial knob formation is a taphonomic quality of the Mühlheim locality.

?Carpal (Figs 4, 5A, A', 6, 8). Adjacent to the distal fifth of the right radius, there is a roughly sub-quadratic bone fragment. Due to its shortness as preserved, it likely represents one of the proximal carpal bones, possibly the radiale. Unfortunately, the preservation of the carpal is too poor for an exact identification. While the assumed proximal face of the carpal is exposed and abraded, its respective distal face, which is embedded in matrix and, thus, only visible in the tomography (Figs. 5A, A'), is preserved in three dimensions. On its assumed anterior face, there is a rounded process that covers half the anterior margin of the bone and is overlain by the radius (Figs 5A, A'). On the respective anterodistal corner of the bone, a pointed triangular process arises, which has barely half the height of the anteroproximal one and covers about one-sixth of the anterior face of the bone. The assumed anterior face between the two processes is deeply concave. This concavity might have accommodated the distal articular end of the radius. The assumed proximal face of the carpal bears a shallow depression.

Metacarpals (Figs 4, 5A, A' 6, 8). The proximal parts of the right metacarpals (mc) II and III are preserved in dorsal aspect. Mc II is about one-third thicker than mc III. The distal third of both bones is missing. Mc II is proximally ovelain by the distal articular head of the radius. Mc III is distally partially overlain by the basal phalanx of digit I. The shaft of mc II bears a longitudinal impaction furrow on its dorsal side. The proximal head of mc III is a transverse ovoid joint, which is angled at about 94° against the shaft in the posterior direction. That of mc II is partially broken and covered by sediment. Nothing more can be said because the bones are badly crushed.

Phalanges (Figs 4, 5A, A', 6, 8, 14). Of digit I, about two-thirds of the proximal portion of the first phalanx are preserved in dorsal aspect. The bone bears a fine longitudinal impaction furrow on the dorsal side (see below, Fig. 14). The proximal articular facet of phalanx I-1 is orientated perpendicularly with respect to the shaft and is set off by a blunt flange, which is one-third wider than the

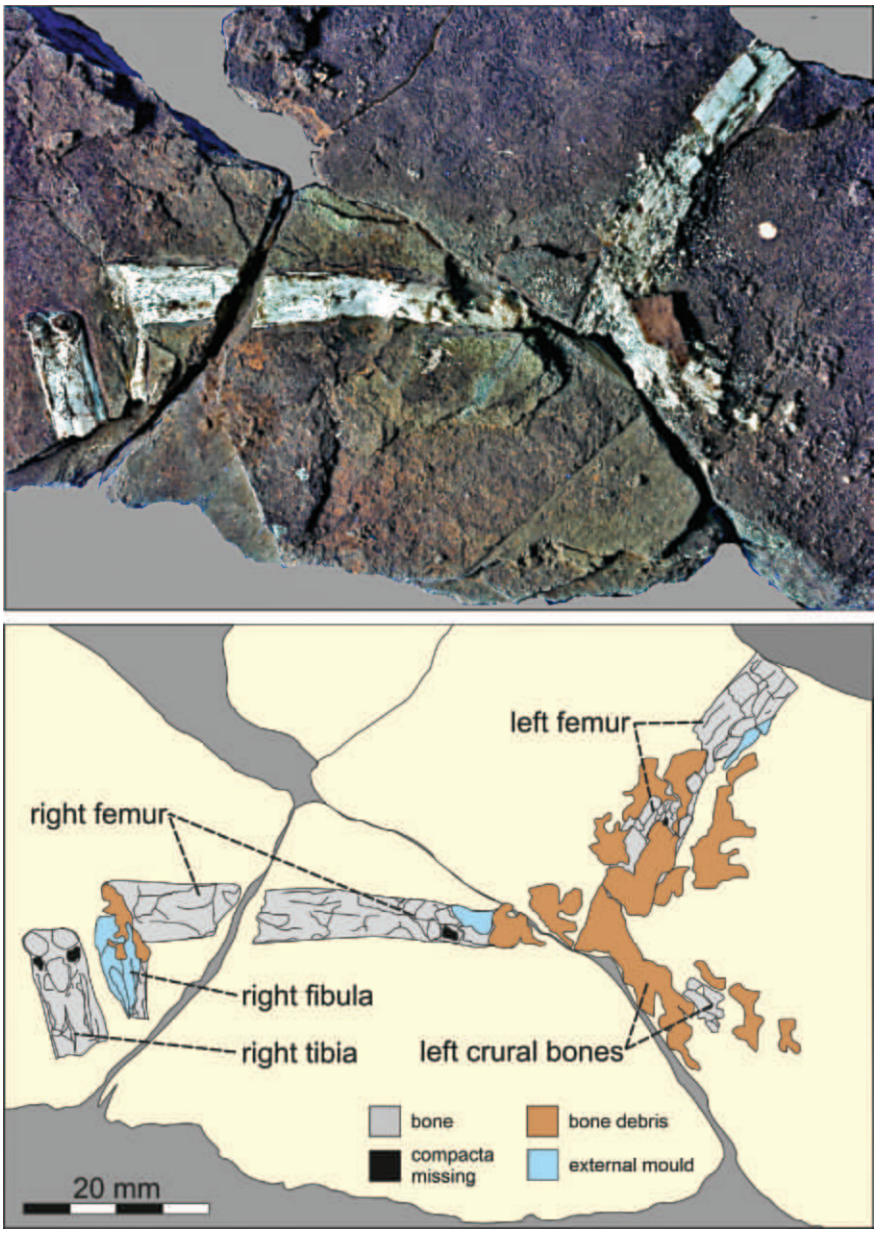

Figure 10. SMNK-PAL 10,000c, hind limbs. Top: under filtered UV light; bottom: interpretive drawing.

distally adjacent part of the shaft. The posterior half of the distal extremity of the articular face is slightly abraded. The proximal articular head is separated into two condyles by a sulcus that continues as a groove with converging margins on to the undamaged part of the shaft and finally vanishes in a fracture zone. The posterior condyle is visible in posterior aspect and is evenly rounded.

The penultimate phalanx of digit II is completely preserved and seen in lateral aspect, in which the palmar surface is facing away from the radius. It is 19 mm long. The proximal articulation facet is slightly expanded in the palmar direction. The shaft is slightly bent dorsally in its distal third. Like in the other manual bones, longitudinal grooves on the shaft are visible, but are the result of diagenetic impaction. The reconstructed cross-section of the mid-shaft of this phalanx was almost circular (Figs 6, 8, 14, ventral impaction furrow faintly also seen in Fig. 5A'). The distal third of the phalanx is strongly compacted. Its end bears a ginglymus, which is abraded. Laterally, a large ligament pit is present.

A manual ungual is exposed in lateral aspect on the lateral side of the distal humerus. The proximal articular facet of the ungual is missing, including part of the flexor tubercle, so that standard measurements cannot be taken. The preserved portion has a maximum length of 9.8 mm. However, even this partial length suggests that this ungual is too large to belong to manual digit I or III (9.2 and 6.7 mm long in the similarly sized Munich specimen; Foth and Rauhut (2017)) and its closer proximity to penultimate phalanx II corroborates this identity. A chisel mark pierces the dorsal margin of the ungual level with the flexor tubercle. Additionally, the proximal third of the ungual is compacted. The proximodorsal edge is covered by the humerus. Due to damage in this region, the tomography scans cannot confirm if an ungual lip was present. The ungual is strongly curved, with an aperture

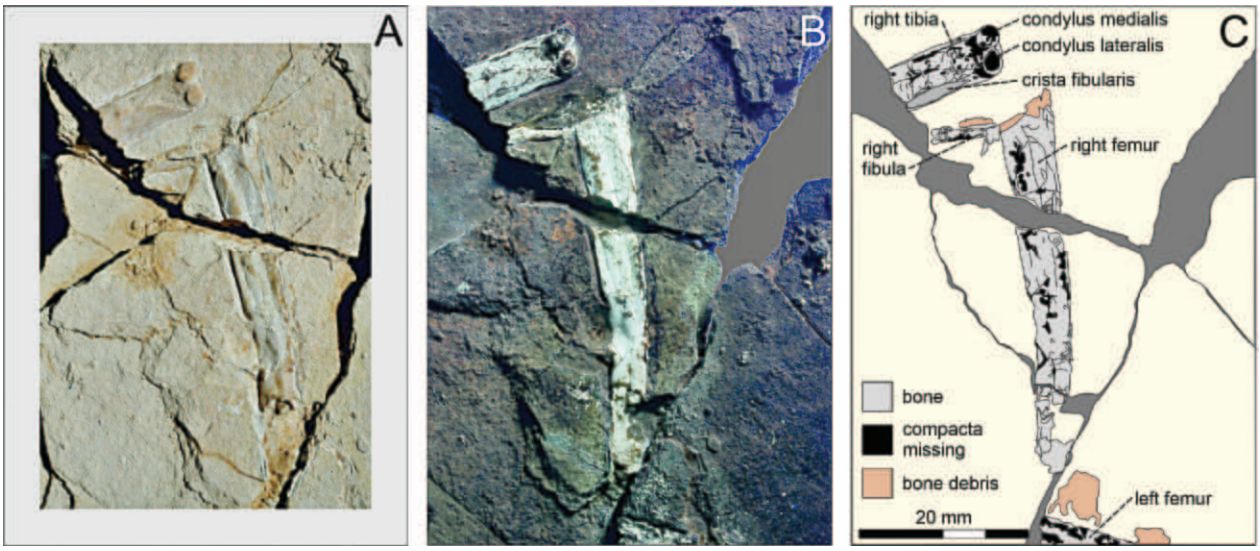

Figure 11. SMNK-PAL 10,000c, right hind limb. **A.** Under natural light; **B.** Under filtered UV light; **C.** Interpretive drawing.

angle of the claw arcade being 110°. The lateral furrow as preserved begins proximally in the ventral third and runs parallel to the ventral margin of the bone. It terminates at the dorsal margin of the ungual close to its tip. There are no remains of a keratinous sheath.

The PCA (Fig. 15A) demonstrates high variability in the morphology of manual unguals in *Archaeopteryx* and *Anchiornis*. The greatest factors of variation amongst the specimens included in this analysis (PC1: 51.13%, PC2: 22.39%) correspond to curvature, dorsoventral height, position of the proximal extent of the dorsal curvature and the morphology of the flexor tubercle. Although these characteristics explain more than 70% of the total morphological variance captured by the landmarks used here, there is pronounced overlap in morphospace. This demonstrates that there is more intrataxonomic than intertaxonomic variation and suggests that curvature, height, position of the ungual lip and flexor tubercle morphology may make poor characters for taxonomic assignment in these taxa.

Due to the high level of intraspecific variation regarding the morphology of the manual unguals, a CDA is required to separate taxonomic groups based on ungual shape (Fig. 15B). The analysis conducted here diagnoses the Karlsruhe specimen as having stronger affinities for *Archaeopteryx* than *Anchiornis*. The same is true for the Mühlheim (*Alcmonavis*) and Haarlem (*Ostromia*) specimens. The manual unguals of *Anchiornis* are characterised by a shallower ungual curvature, a more distally positioned flexor tubercle and being proximodistally shorter. The manual unguals of *Archaeopteryx* are characterised by a deeper ungual curvature, a more proximally positioned flexor tubercle and being proximodistally longer.

Hind limbs (Figs 5C, C', D, D', 10, 11). The shafts of both femora are preserved, but the articular ends are missing in both elements. Both femoral shafts show a slight medial curvature. The distal half of the shaft of the left femur is pulverised (Figs 5D, D', 11). The cnemial area is devoid of any identifiable structure. Remains of the left tibial and probably the fibular head, as well as the proximal-most parts of their shafts, are in association with the respective femur.

The better-preserved shaft of the right femur is seen in posterior aspect (Figs 5C, C', 10). The posterior intercondylar sulcus extends about one-third of the shaft. The condylar area is missing as is the proximal articular end of the bone. As preserved, the cnemial articulation is about twice as wide as the narrowest part of the corresponding shaft.

Of the right tibia, only the proximal end is preserved, and is seen in posterior aspect (Figs 5C, C' 10, 11). The condylus medialis is subcircular in outline and a little larger than the transversely oval condylus lateralis. The surface immediately distal to the condyli is impacted. The lateral margin of the tibia is formed by the shallowly concave posterior side of the crista fibularis, which begins shortly distal to the condylus lateralis and is terminated distally by a matrix fracture.

Of the right fibula, only the proximal-most fragment is partially preserved, with the articular head missing (Figs 5C, C', 10, 11). The bone parallels the tibia. Like in the left hind limb, the crural elements are at a right angle with the respective femur.

Discussion

Phylogeny

The phylogenetic analysis of the equally weighted characters resulted in over 200,000 maximum parsimony trees (MPTs) with a length of 3,666 steps (CI: 0.211; RI: 0.733). The strict consensus tree shows a large polytomy of basal coelurosaurs, with Alvarezsauroidea, Therizinosauria, Avialae and subclades of Tyrannosauroidea, Dromaeosauridae, Troodontidae and Ornithomimosauria

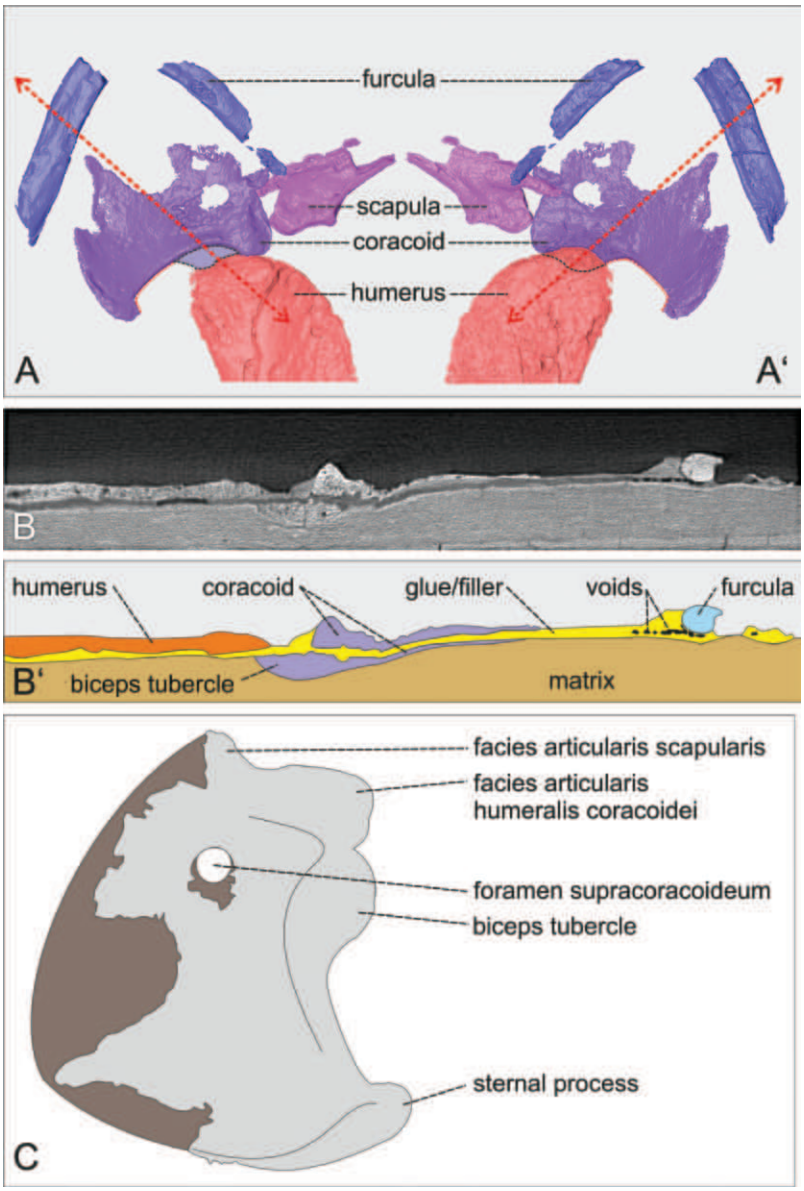

Figure 12. SMNK-PAL 10,000a, shoulder region and coracoid. **A.** Tomography of exposed surface; **A'.** Tomography of surface embedded in the matrix; note that the biceps tubercle (highlighted with dotted line) protrudes beyond the humeral head; the arrows mark the section in **B** and **B'**; **B.** Cross-sectional scan through furcula, coracoid and the humeral head; note that this part of the specimen has split into a thick slab and a thin and brittle counter-slab. Both slabs contained bones and were glued upon each other. Then the matrix of the counter-slab was prepared away; the biceps tubercle underlies the humeral head; **C.** Restoration of the coracoid according to **A, A'** and **B, B'**. Remark on the glue layer.

being partly resolved (Suppl. material 2). After pruning, the polytomy at the base of Coelurosauria remains for non-pennaraptoran taxa, in which the topology of ornithomimosaurs and tyrannosauroids is slightly better resolved. Crownwards, the main clades of Pennaraptora could be recovered, in which Oviraptorosauria represent the sister clade of Paraves. Here, Scansoripterygidae are basal members of Oviraptorosauria (see Agnolín and Novas (2013); Brusatte et al. (2014); Rauhut et al. (2019)) not Paraves (for example, Xu et al. (2015); Wang et al. 2019b) (Fig. 16A, Suppl. materials 2, 3).

Within Paraves, our analysis found the clade Deinonychosauria to be paraphyletic. In contrast to previous analyses showing a paraphyly of this group (for example, Godefroit et al. (2013); Choiniere et al. (2014); Foth et al. (2014); Foth and Rauhut (2017)), Dromaeosauridae and not Troodontidae are now the sister group of Avialae, which was previously only found by Agnolín and Novas (2013). However, in contrast to the latter study, Unenlagiinae and Microraptorinae are still members of the Dromaeosauridae in this analysis and do not represent basal Avialae. Furthermore, the enigmatic dromaeosaurid *Balaur* is a member of Unenlagiinae, while it was previously found to be a Velociraptorinae (for example, Turner et al. (2012); Brusatte et al. (2013)) or basal Avialae (Foth et al. 2014; Cau et al. 2015; Foth and Rauhut 2017). Comparing the current topology with previous analyses shows that the interrelationship within

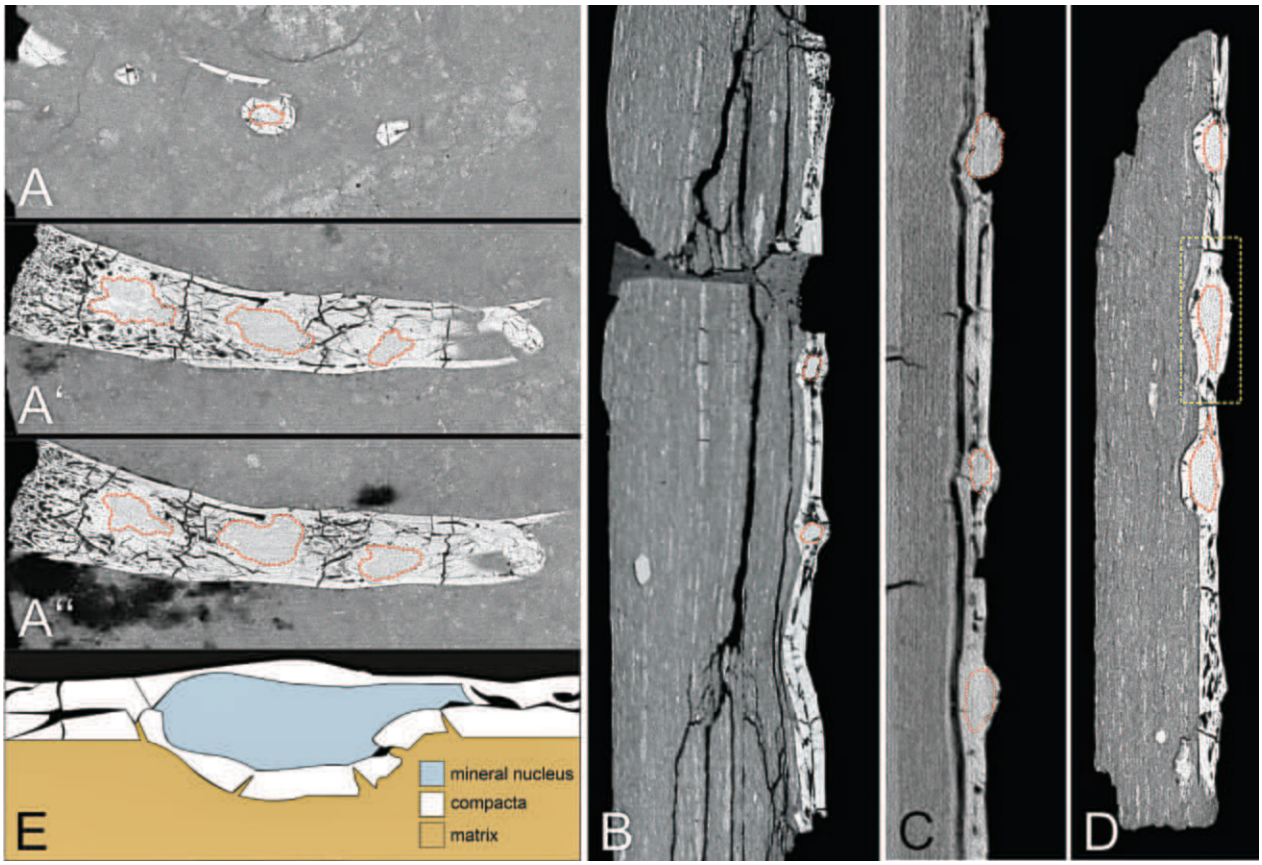

Figure 13. SMNK-PAL 10,000a, longitudinal CT sections through the right ulna and femur. **A-A"**) horizontal sections through the ulna; **B.** Vertical section through the femur; **C, D.** Vertical sections through the ulna; the broken red circles mark the framboidal mineral nucleus that prevented the collapse of the compacta leaving a knob; **E.** line drawing of the middle section of **D** (yellow square).

Paraves still remains controversial (Pol and Goloboff 2020) and depends on taxon and character sampling of early Paraves, which show a generally high level of homoplasy (Rauhut and Foth 2020).

As discovered by Foth and Rauhut (2017), *Ostromia* (Haarlem specimen) is still placed within Anchiornithinae, which represents the earliest branching larger clade within Avialae. Thus, the deletion of the characters referring to longitudinal furrows along the radius, metacarpals and phalanges had no impact on the phylogenetic placement. The position is only supported by the presence of a convex pubic shaft (char. 494). The shaft itself is not preserved in the form of bone, but only as imprints in the rock matrix that suffered some erosion. Given that some *Archaeopteryx* specimens (for example, Munich specimen) show breakages in the pubic shaft (Wellnhofer 2009), we cannot rule out that the curvature represents a potential break. Therefore, this issue requires some further investigation. It should also be noted that the Haarlem specimen's ungual shape does not correspond to that of *Anchiornis*, but, due to its marginal position in the CDA, it is also somehow distinct from the sampled training data of *Archaeopteryx* (Fig. 15B). In addition, the flexor tubercles of both species tend to be somewhat distinct, being more angular in *Ostromia* and rounded in *Archaeopteryx* (although, see the plateaus in the unguals of the Munich and Solnhofen specimens). Given that *Ostromia* and *Anchiornis* lived in different habitats and continents, this disparity could reflect ecological adaptations and/or genetic drift. *Pedopenna* and *Xiaotingia* are not members of Anchiornithinae, but placed more stemwards within Avialae (see also Rauhut et al. (2019)).

According to our phylogenetic analysis, SMNK-PAL 10,000 is found in a polytomy with *Archaeopteryx* and lacks any autapomorphic characters that distinguish it from the latter. Character 428 (manual phalanx I-1) is the only one out of 78 characters, wherein the new specimen (0/straight) differs from *Archaeopteryx* (1/bowed, palmar surface concave). However, given the strong compression in the dorsopalmar direction, a taphonomic artefact cannot be ruled out for the flat nature of this bone. Both OTUs are sister to the clade including *Alcmonavis* and Euavialae (the clade containing *Jixiangornis*, *Jeholornis* and *Passer domesticus* and all descendants of their most recent common ancestor, see Ji et al. (2002)) (Fig. 16A).

For the implied weighted characters, the phylogenetic analysis resulted in over 13,365 MPTs with a length of 3,676 steps (Best Score: 157.511; CI: 0.211; RI: 0.732). The strict consensus tree also bears a large polytomy with Alvarezsauroidea, Therizinosauria and subclades of Tyrannosauroidea, Paraves, Oviraptorosauria, Troodontidae and Ornithomimosauria that are partly resolved (Suppl. material 2). Like in the first analysis, Dromaeosauridae

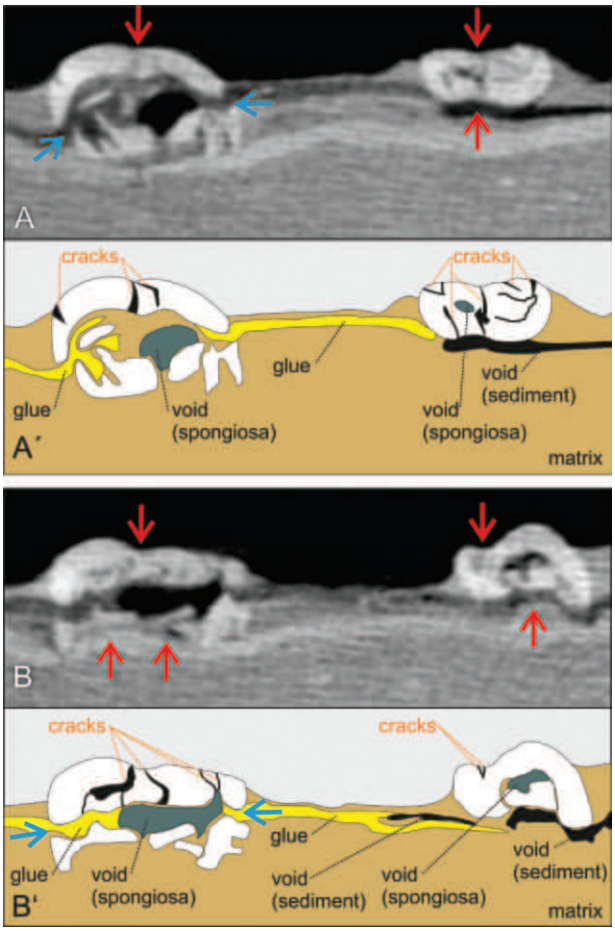

Figure 14. SMNK-PAL 10,000a, CT sections through the right radius and the penultimate phalanx of the right digit II. **A.** CT section 1 according to Fig. 8A. **A'.** line drawing of CT section 1; **B.** CT section 2 according to Fig. 8A. **B'.** line drawing of CT section 2; Note that the "furrows" are generated by compaction (red arrows) that caused linear cracks along the long axes of the bones with the medullar cavity still being mostly hollow. The bones must have been fixed in the matrix prior to compaction, because the bone parts did not separate from each other. The radius might have been subject to an internal pressure that caused a separation of the upper and lower bone elements (blue arrows).

are the sister clade of Avialae. In the reduced consensus tree (Fig. 16B, Suppl. materials 2, 3), Tyrannosauroidea (including *Coelurus*, *Sinocalliperyx*, *Tanyclolagreus* and *Xumenglong*) represent the most basal clade of coelurosaurs. *Zuolong* has a more crownward position than in previous analyses (see, for example, Choiniere et al. (2014); Brusatte et al. (2014)), representing the sister taxon of the clade including Compsognathidae and Maniraptoriformes. The fragmentary *Aniksosaurus* and *Tugulusaurus* represent basal ornithomimosaurs. As proposed by Hattori et al. (2022), *Fukuivenator* represents a basal therizinosaur. In contrast to many previous phylogenetic analyses (for example, Turner et al. (2012); Brusatte et al. (2014); Foth et al. (2014); Wang et al. (2019b)), Alvarezsauroidea are the sister clade to Pennaraptora (including *Yixianosaurus*), being more crownwards than therizinosaurs (see Zanno (2010)). Like in the previous analysis, SMNK-PAL 10,000 is recovered as basal Avialae in a polytomy with *Archaeopteryx*.

If the main topology is held constant, adding *Ostromia* to the polytomy of SMNK-PAL 10,000 and *Archaeopteryx* requires one step (implied weight: +1 step). A monophyletic group including SMNK-PAL 10,000, *Archaeopteryx* and *Alcmonavis* within Avialae requires two additional steps (implied weight: +2 steps), while the grouping of all Solnhofen OTUs into one monophylum makes the tree three steps longer (implied weight: +3 steps). A placement of SMNK-PAL 10,000 at the base of Dromaeosauridae requires four additional steps (implied weight: +4 steps) and five additional steps for a placement at the base of Troodontidae (implied weight: +5 steps). A sister-group relationship between Troodontidae and Avialae (for example, Godefroit et al. (2013); Foth et al. (2014); Foth and Rauhut (2017)) requires nine additional steps (implied weight: +3 steps). In contrast, monophyletic Deinonychosauria (for example, Clark et al. (2002); Hu et al. (2009); Turner et al. (2012); Brusatte et al. (2014)) requires seven additional steps (implied weight: +5 steps) and is, thus, less likely than the other two alternatives. A placement of Anchiornithinae at the base of Troodontidae (for example, Hu et al. (2009); Turner et al. (2012); Brusatte et al. (2014)) requires 20 additional steps if Troodontidae are the sister group of Avialae (implied weight: +16 steps) and one step more (21 steps) if Dromaeosauridae are the next relatives to Avialae (implied weight: +17 steps). If Microraptorinae and Unenlagiinae represent basal Avialae, as proposed by Agnolín and Novas (2013), the tree becomes 28 steps longer (implied weight: +26 steps). In contrast, placing SMNK-PAL 10,000 together with anchiornithines, *Archaeopteryx* and *Alcmonavis* within Deinonychosauria (for example, Xu et al. (2011); Xu et al. (2015); Hu et al. (2018)) results in trees that are at least 39 steps longer than the most parsimonious trees (implied weight: +34 steps), depending on the placement of *Pedopenna* and *Xiaotingia* as basal Deinonychosauria or Avialae. Thus, most of the tested alternative phylogenetic hypotheses for the inner relationships of Paraves are rather unlikely.

Ungual geometry

The manual unguals of *Archaeopteryx* and *Anchiornis* show a tremendous amount of morphological variation, similar to what is seen in modern birds (Hedrick et al. 2019). Previous studies of the unguals of *Archaeopteryx* and *Anchiornis* (Cobb and Sellers 2020) have also had difficulty with the high degree of variability found. This variation makes diagnosing taxonomic identity difficult without specialised statistical tools. The high degree of variation exacerbates issues like small sample sizes, taphonomic effects, non-orthogonal photos and human error. As such, caution should be taken when drawing conclusions based solely on ungual morphology.

Nevertheless, the unguals of *Archaeopteryx* and *Anchiornis* are morphologically distinct as indicated by the two well-separated clusters in the CDAs of all digits (Fig. 15B) and only digit II (Fig. 15D). As the Karlsruhe, Haarlem and Mühlheim specimens have been added to the CDA passively as "mystery specimens", they naturally cluster less tightly than those specimens actively contributing to the given separation between *Archaeopteryx* and *Anchiornis*. Unguals III and II of the Haarlem and Mühlheim specimens, respectively, are the least *Anchiornis*-like in the dataset. Ungual II of the Karlsruhe specimen lies between *Archaeopteryx* and *Anchiornis*, but much closer to the former. However, we cannot rule out that the taphonomic damage (compaction) to the flexor tubercle in the Karlsruhe specimen is responsible for a rightward shift along the axis (Fig. 15B; i.e. relatively distal tubercle compared to the rest of the *Archaeopteryx* specimens). Ungual III of the Haarlem specimen is located to the left outside of the *Archaeopteryx* cluster.

Limiting the analysis to only ungual II of *Archaeopteryx* and *Anchiornis* shows that the variation exhibited by all unguals is not the same as that exhibited by only ungual II (Fig. 15C). In this PCA, the Karlsruhe specimen plots more within the morphospace exhibited by *Archaeopteryx* than in Fig. 15A, although there is still significant overlap between the morphospace of *Archaeopteryx* and *Anchiornis*. The CDA illustrates that ungual II of the Karlsruhe specimen has a strong morphological affinity with *Archaeopteryx* (Fig. 15D) and much stronger than when comparing all unguals (Fig. 15B).

Systematic palaeontology

Due to the fragmentary nature of the new specimen, comparison with other Avialae from the fossil assemblage of the Late Jurassic Solnhofen Archipelago is difficult. As is seen on the mould on the counter-slab of TM 6929, *Ostromia* possesses a longitudinal furrow on the radius

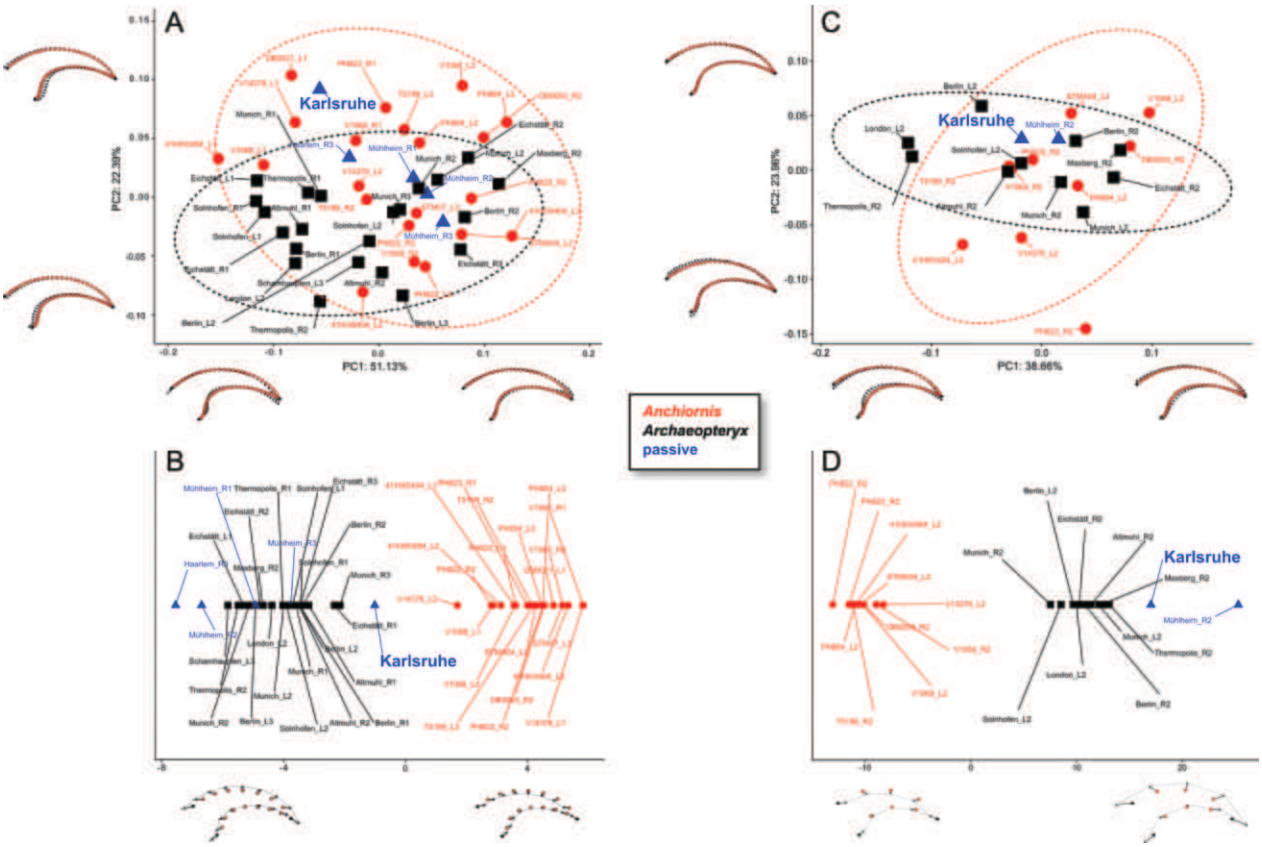

Figure 15. Geometric Morphometric Analysis for manual unguals of Urvögel (*Archaeopteryx* and passive) and *Anchiornis* specimens. **A.** Principal Component Analysis (PCA); PC1 primarily corresponds to curvature, position of the proximal base of the dorsal curvature and curvature of the flexor tubercle; PC2 primarily corresponds to dorsoventral height and proximodistal position of the flexor tubercle; **B.** Canonical Discriminant Analysis (CDA) discriminating between the manual unguals of *Anchiornis* and *Archaeopteryx*. **C.** PCA for manual unguals from only digit II; PC1 primarily corresponds to curvature of the flexor tubercle; PC2 primarily corresponds to dorsoventral height. **D.** CDA discriminating between the manual unguals from only digit II of *Anchiornis* and *Archaeopteryx*; the reduced number of semi-landmarks is due to smaller sample sizes. The "passive" group was included in the analysis passively, such that their morphology does not influence the discrimination; as such, they will also cluster more loosely with either group. Each of the passive specimens (Karlsruhe, Haarlem and Mühlheim) show greater taxonomic affinities for *Archaeopteryx* than for *Anchiornis*. Thin-plate splines are used to illustrate the morphology at each extreme end of each axis. Black dots represent landmarks and red dots represent semi-landmarks.

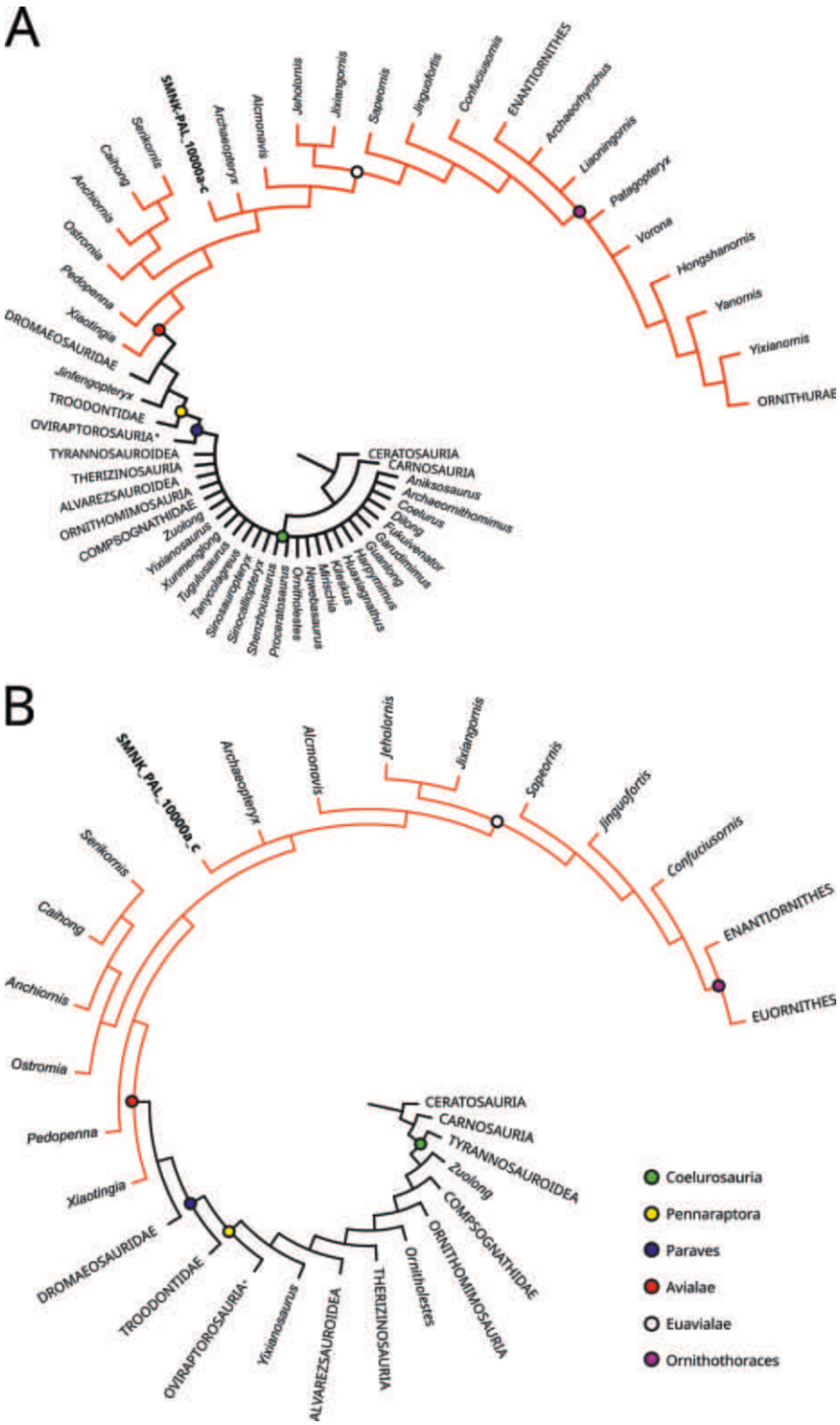

Figure 16. Phylogenetic position of SMNK-PAL 10,000a-c. **A.** Reduced consensus tree under equal weight; **B.** Reduced consensus tree under implied weight (see Materials and Methods and Suppl. materials 1–5 for details).

and on the smanual phalanx I-1 (Foth and Rauhut 2017). However, the furrow-like structures that are seen on the respective bones of SMNK 10,000 (Figs 5A, 6, 8, 9) are due to impaction (Fig. 14), while the interpretation of the situation in *Ostromia* is not clear and requires a CT-based follow-up examination (Mulder et al. 2024). Ungual II of the new specimen is a little less curved than ungual III of *Ostromia* (Fig. 15A). Whether or not *Ostromia* possesses a tuberculum bicipitale radii cannot be evaluated. Like *Alcmonavis* and some other specimens of *Archaeopteryx* (Rauhut et al. 2019), SMNK PAL 10,000 shares the presence of a tuberculum bicipitale radii (Fig. 5A'). However, the tubercle is more pronounced in *Alcmonavis*. The angle in the proximal third of the humeral shaft in SMNK

PAL 10,000 is about 5° greater than in *Alcmonavis*, but similar to the angulation seen in the London and Daiting specimens of *Archaeopteryx*. The tomography scans further reveal that an anteromedially inclined facet for the attachment of the m. pectoralis on the deltopectoral crest is absent in SMNK PAL 10,000 (Fig. 5A).

Although none of the diagnostic features (or combination of diagnostic features) of the genus *Archaeopteryx* (see Rauhut et al. (2018); Kundrát et al. (2019)) is preserved in the new specimen, the phylogenetic analyses support an assignment to this genus. Like *Archaeopteryx*, SMNK PAL 10,000 bears an offset sternal process on the distal end of the coracoid (Figs 5–7, 12), an angle between the furcular rami of about 80° (similar to that of the London, Thermopolis and Daiting specimens; de Beer (1954); Carney (2016); Kundrát et al. (2019)), an angle between in the proximal third of the humeral shaft of about 30°, the absence of an attachment facet of m. pectoralis on the medial side of the deltopectoral crest and a small triangular tuberculum bicipitale radii on the proximal end of the radius (Figs 5A', 9A–A''). Finally, ungual II has a much stronger morphological affinity to *Archaeopteryx* than to *Anchiornis* (Fig. 15B, D).

Based on its humeral length, the specimen is within the size range of the Daiting, Munich, Thermopolis and "chicken wing" specimens (Mayr et al. 2007; Wellnhofer 2009; Kundrát et al. 2019) and, thus, represents one of the medium-sized specimens.

Taphonomy

The radius, metacarpal II and phalanges of digit I and II bear longitudinal furrows (Figs 6, 8, 9). CT sections show that these furrows are the results of a late diagenetic compaction (Fig. 14). The compaction furrows on the contralateral radii are topographically identical, suggesting that the compaction effect was subject to the mechanical properties of a hollow bone tube. If this is the case, the phylogenetic importance of these furrows, which are also seen in, for example, *Ostromia*, *Alcmonavis*, *Anchiornis* (Foth and Rauhut 2017; Rauhut et al. 2019) and some Euavialae (Chiappe and Walker 2002; Sanz et al. 2002; Hu et al. 2015; Li et al. 2023) should be re-investigated in the light of taphonomy, especially if the fossils suffered heavy compression during diagenesis (see, for example, Mulder et al. (2024)). Apparently, SMNK PAL 10,000 underwent two major phases of diagenesis. The first phase comprised a superficial embedding of the hollow bones. Inside both ulnae, mineral precipitation occurred, which was only possible as long as these bones were unaffected by compression and filled with water. The second phase started with the compression of the sediment with the bone still being water-filled. If the diameter of the hollow shafts was thin and the compacta thick with respect to the diameter, as is the case in the mid-shaft of the radius and the phalanges, the compressed sediment stabilised the bone walls and the hollow shaft was impacted along the highest point of the tube. If so, the compaction probably changed the bone diameter only slightly. In areas with greater diameters and respectively thin bone walls, the sediment compression resulted in a compaction of the hollow bones. Only the crystal cores inside the ulnae resisted this compaction, leading to the formation of the circular knobs described (Fig. 13).

The mechanics of compaction and impaction of hollow bones should be experimentally reconstructed with actuopalaeontological methods, which is beyond the scope of this paper. However, the interpretation of morphological structure of both fossilised hard and soft tissues should be carefully cross-checked for possible taphonomic or diagenetic effects (see, for example, Foth (2012)). This is especially significant for morphologies with potential phylogenetic or diagnostic meaning. In this light, some of the diagnostic characters of *Archaeopteryx albersdoerferi* described by Kundrát et al. (2019) may also be artefacts, because the Daiting specimen also suffered heavy compression during fossilisation. Until now, only five CT studies of the osteology of *Archaeopteryx* and *Ostromia* have been conducted (Carney 2016; Voeten et al. 2018, 2024; Kundrát et al. 2019; Mulder et al. 2024). Further studies are required to investigate the diagenesis of specimens and separate morphological facts from taphonomic artefacts.

Conclusions

The new *Archaeopteryx* specimen SMNK PAL 10,000 from the Franconian Alb described herein is the second avialan theropod after *Alcmonavis poeschli* reported from the Lower Tithonian Mörnsheim Formation at Mühlheim, the third from the Lower Tithonian Mörnsheim Formation and, according to Rauhut et al. (2018), the twelfth specimen that represents the genus. Although the fossil preservation of SMNK PAL 10,000 is rather poor, an assignment to *Archaeopteryx* sp. is supported by a morphological comparison with *Archaeopteryx*, *Alcmonavis* and *Ostromia*, as well as the phylogenetic and GMM analyses. However, the investigation of the remains of SMNK PAL 10,000 revealed that taphonomy, diagenesis and the material properties of hollow bones under pressure could result in morphological artefacts that may substantially confuse taxonomic and phylogenetic surveys. The exclusion of characters related to the longitudinal furrows (in the radius, metacarpals and manual phalanges) that may result from such collapses did not affect the phylogenetic positions of *Ostromia* and *Alcmonavis*. Ultimately, however, a comprehensive specimen-based analysis of all Urvögel is sorely needed to definitively resolve the controversial taxonomy of these iconic paravians.

Data availability

All files related to the phylogenetic and geometric morphometric analyses are attached as supplementary files. The tomographic datasets are deposited for download at the RADAR4KIT archive of Karlsruhe Institute of Technology (https://dx.doi.org/10.35097/uKocWRJSpEoneZtN). The landmark files can be found at Zenodo (https://doi.org/10.5281/zenodo.12700175).

Acknowledgements

The authors gratefully acknowledge the data storage service SDS@hd supported by the Ministry of Science, Research and the Arts Baden-Württemberg (MWK), the German Research Foundation (DFG) through grant INST 35/1503-1 FUGG (TvdK, MZ and EH) and the Swiss National Science Foundation (PZ00P2_174040 to CF). We are also grateful to the management of the 'Besuchersteinbruch Mühlheim' (Visitors' Quarry Mühlheim), where the specimen was found and secured for science. For the preparation, we wish to thank Ulrich Leonhardt (Creuzburg, Germany). We also thank Julian Kimmig for generous access to the specimen and Tim Niggemeyer (Karlsruhe, Germany) for his sophisticated post-preparation of the shoulder area. Our special thanks go to 'Freunde des Naturkundemuseums Karlsruhe e.V.' (Friends of the Natural History Museum Karlsruhe), who financially supported the acquisition of the specimen. Finally, we thank Tom Holtz and Dennis Voeten for their critical comments, which helped to improve the earlier version of the manuscript.

References

Adams D, Collyer M, Kaliontzopoulou A, Baken E (2023) *Geomorph*: Software for geometric morphometric analyses. *R* package version 4.0.6. https://cran.r-project.org/web/packages/geomorph/index.html

Albersdörfer R, Häckel, W (2015) Die Kieselplattenkalke von Painten. In: Arratia G, Schultze H-P, Tischlinger H, Viohl G (Eds) Solnhofen – Ein Fenster in die Jurazeit. Verlag Dr. Friedrich Pfeil, München, 126–133.

Agnolín FL, Novas FE (2013) Avian Ancestors. A Review of the Phylogenetic Relationships of the Theropods Unenlagiidae, Microraptoria, *Anchiornis* and Scansoriopterygidae. Springer, Dordrecht, 96 pp. https://doi.org/10.1007/978-94-007-5637-3

Agnolín FL, Motta MJ, Egli FB, Lo Coco G, Novas FE (2019) Paravian phylogeny and the dinosaur-bird transition: an overview. Frontiers in Earth Science 6: 252. https://doi.org/10.3389/feart.2018.00252

Arratia G, Schultze, H-P, Tischlinger H, Viohl G (2015) Solnhofen – Ein Fenster in die Jurazeit. Verlag Dr. Friedrich Pfeil, München, 620 pp.

Balter M (2013) Authenticity of China's fabulous fossils gets new scrutiny. Science 340: 1153–1154. https://doi.org/10.1126/science.340.6137.1153

de Beer G (1954) *Archaeopteryx lithographica*: A Study Based upon the British Museum Specimen. British Museum (Natural History), London, 68 pp.

Brusatte SL, Vremir M, Csiki-Sava Z, Turner AH, Watanabe A, Erickson GM, Norell MA (2013) The osteology of *Balaur bondoc*, an island-dwelling dromaeosaurid (Dinosauria: Theropoda) from the Late Cretaceous of Romania. Bulletin of the American Museum of Natural History 374: 1–100. https://doi.org/10.1206/798.1

Brusatte SL, Lloyd GT, Wang SC, Norell MA (2014) Gradual assembly of avian body plan culminated in rapid rates of evolution across the dinosaur-bird transition. Current Biology 24: 2386–2392. https://doi.org/10.1016/j.cub.2014.08.034

Burnham DA (2004) New information on *Bambiraptor feinbergi* (Theropoda: Dromaeosauridae) from the Late Cretaceous of Montana. In: Currie PJ, Koppelhus EB, Shugar MA, Wright JL (Eds) Feathered Dragons. Indiana University Press, Bloomington, 67–111.

Carney RM (2016) Evolution of the archosaurian shoulder joint and the flight stroke of *Archaeopteryx*. PhD Thesis, Brown University, Providence, U.S.A.

Carney RM, Tischlinger H, Shawkey MD (2020) Evidence corroborates identity of isolated fossil feather as a wing covert of *Archaeopteryx*. Scientific Reports 10: 15593. https://doi.org/10.1038/s41598-020-65336-y

Cau A, Brougham T, Naish D (2015) The phylogenetic affinities of the bizarre Late Cretaceous Romanian theropod *Balaur bondoc* (Dinosauria, Maniraptora): dromaeosaurid or flightless bird? PeerJ 3: e1032. https://doi.org/10.7717/peerj.1032

Chiappe LM, Walker CA (2002) Skeletal morphology and systematics of the Cretaceous Euenantiornithes (Ornithoraces: Enantiornithes). In: Chiappe LM, Witmer LM (Eds) Mesozoic Birds: Above the Heads of Dinosaurs. University of California Press, Berkeley, 240–267.

Chiappe LM, Meng Q (2016) Birds of Stone: Chinese Avian Fossils from the Age of Dinosaurs. Johns Hopkins University Press, Baltimore, 294 pp.

Chiappe LM, Ji S, Ji Q, Norell MA (1999) Anatomy and systematics of the Confuciusornithidae (Theropoda: Aves) from the late Mesozoic of northeastern China. Bulletin of the American Museum of Natural History 242: 1–89.

Choiniere JN, Clark JM, Forster CA, Norell MA, Eberth DA, Erickson GM, Chu H, Xu X (2014) A juvenile specimen of a new coelurosaur (Dinosauria: Theropoda) from the Middle–Late Jurassic Shishugou Formation of Xinjiang, People's Republic of China. Journal of Systematic Palaeontology 12: 177–215. https://doi.org/10.1080/14772019.2013.781067

Clark JM, Norell MA, Makovicky PJ (2002) Cladistic approaches to the relationships of birds to other theropod dinosaurs. In: Chiappe LM, Witmer LM (Eds) Mesozoic Birds: Above the Heads of Dinosaurs. University of California Press, Berkeley, 31–61.

Cobb SE, Sellers WI (2020) Inferring lifestyle for Aves and Theropoda: a model based on curvatures of extant avian ungual bones. PLoS ONE 15: e0211173. https://doi.org/10.1371/journal.pone.0211173

Faragó T, Gasilov S, Emslie I, Zuber M, Helfen L, Vogelgesang M, Baumbach T (2022) *tofu*: a fast, versatile and user-friendly image processing toolkit for computed tomography. Journal of Synchrotron Radiation 29: 916–927. https://doi.org/10.1107/S160057752200282X

Foth C (2012) On the identification of feather structures in stem-line representatives of birds: evidence from fossils and actuopalaeontology, Paläontolologische Zeitschrift 86: 91–102. https://doi.org/10.1007/s12542-011-0111-3

Foth C, Rauhut OWM (2017) Re-evaluation of the Haarlem *Archaeopteryx* and the radiation of maniraptoran theropod dinosaurs. BMC Evolutionary Biology 17: 236. https://doi.org/10.1186/s12862-017-1076-y

Foth C, Tischlinger H, Rauhut OWM (2014) New specimen of *Archaeopteryx* provides insights into the evolution of pennaceous feathers. Nature 511: 79–82. https://doi.org/10.1038/nature13467

Gauthier JA (1986) Saurischian monophyly and the origin of birds. Memoirs of the Californian Academy of Science 8: 1–55.

Gianechini FA, Makovicky PJ, Apesteguía S, Cerda IA (2018) Postcranial skeletal anatomy of the holotype and referred specimens of *Buitreraptor gonzalezorum* Makovicky, Apesteguía and Agnolín 2005 (Theropoda, Dromaeosauridae), from the Late Cretaceous of Patagonia. PeerJ 6: e4558. https://doi.org/10.7717/peerj.4558

Godefroit PA, Cau A, Hu D, Escuillié F, Wenhao W, Dyke G (2013) A Jurassic avialan dinosaur from China resolves the early phylogenetic history of birds. Nature 498: 359–362. https://doi.org/10.1038/nature12168

Goloboff PA, Morales ME (2023) *TNT* version 1.6 with a graphical interface for *MacOX* and *Linux*, including new routines in parallel. Cladistics 39: 144–153. https://doi.org/10.1111/cla.12524

Goloboff PA, Torres A, Arias JS (2018) Weighted parsimony outperforms other methods of phylogenetic inference under models appropriate for morphology. Cladistics 34: 407–437. https://doi.org/10.1111/cla.12205

Guo X, Xu L, Jia S (2018) Morphological and phylogenetic study based on new materials of *Anchiornis huxleyi* (Dinosauria, Theropoda) from Jianchang, Western Liaoning, China. Acta Geologica Sinica - English Edition 92: 1–15. https://doi.org/10.1111/1755-6724.13491

Hattori S, Kawabe S, Mai T, Shibata M, Miyata K, Xu X, Azuma V (2022) Osteology of *Fukuivenator paradoxus*: a bizarre maniraptoran theropod from the Early Cretaceous of Fukui, Japan. Memoir of the Fukui Prefectural Dinosaur Museum 20: 1–82.

Hedrick BP, Cordero SA, Zanno LE, Noto C, Dodson P (2019) Quantifying shape and ecology in avian pedal claws: the relationship between the bony core and keratinous sheath. Ecology and Evolution 9: 11545–11556. https://doi.org/10.1002/ece3.5507

Heilmann G (1926) The Origin of Birds. H.F. & G. Witherby, London, 208 pp.

Heyng AM, Leonhardt U, Krautworst U, Pöschl R (2011) Fossilien der Mörnsheim-Formation am Schaudiberg. Fossilien Sonderheft 2011: 22–35.

Heyng AM, Leonardt U, Krautworst U, Pöschl R (2015) Die Mörnsheimer Schichten am Schaudiberg. In: Arratia G, Schultze H-P, Tischlinger H, Viohl G (Eds) Solnhofen – Ein Fenster in die Jurazeit. Verlag Dr. Friedrich Pfeil, München, 137–152.

Hone DWE, Lauer R, Lauer B, Spindler F (2023) *Petrodactyle wellnhoferi* gen. et sp. nov.: a new and large ctenochasmatid pterosaur from the Late Jurassic of Germany. Palaeontologia Electronica 26: a25. https://doi.org/10.26879/1251

Hu D, Hou L, Zhang L, Xu X (2009) A pre-*Archaeopteryx* troodontid theropod from China with long feathers on the metatarsus. Nature 461: 640–643. https://doi.org/10.1038/nature08322

Hu D, Liu Y, Li J, Xu X, Hou L (2015) *Yuanjiawaornis viriosus*, gen. et sp. nov., a large enantiornithine bird from the Lower Cretaceous of western Liaoning, China. Cretaceous Research 55: 210–219. https://doi.org/10.1016/j.cretres.2015.02.013

Hu D, Clarke JA, Eliason CM, Qiu R, Li Q, Shawkey MD, Zhao C, D`Albla L, Jiang J, Xu X (2018) A bony-crested Jurassic dinosaur with evidence of iridescent plumage highlights complexity in early paravian evolution. Nature Communications 9: 217. https://doi.org/10.1038/s41467-017-02515-y

Huxley T (1868) On the animals which are most nearly intermediate between birds and reptiles. Annals and Magazin of Natural History 4: 66–75.

Ji Q, Ji S, Zhang H, You H, Zhang J, Wang L, Yuan C, Ji X (2002) A new avialan bird – *Jixiangornis orientalis* gen. et sp. nov. – from the Lower Cretaceous of western Liaoning, NE China. Journal of Nanjing University (Natural Sciences) 38: 723–736.

Kundrát M, Nudds J, Kear BP, Lü J, Ahlberg P (2019) The first specimen of *Archaeopteryx* from the Upper Jurassic Mörnsheim Formation of Germany. Historical Biology 31: 3–63. https://doi.org/10.1080/08912963.2018.1518443

Lefèvre U, Cau A, Cincotta A, Hu D, Chinsamy A, Escuillié F, Godefroit P (2017) A new Jurassic theropod from China documents a transitional step in the macrostructure of feathers. The Science of Nature 104: 74. https://doi.org/10.1007/s00114-017-1496-y

Li Z, Wang M, Stidham TA, Zhou Z (2023) Decoupling the skull and skeleton in a Cretaceous bird with unique appendicular morphologies. Nature Ecology & Evolution 7: 20–31. https://doi.org/10.1038/s41559-022-01921-w

Lindgren J, Sjövall P, Carney RM, Cincotta A, Uvdal P, Hutcheson SW, Gustafsson O, Lefèvre U, Escuillié F, Heimdal J, Engdahl A, Gren JA, Kear BP, Wakamatsu K, Yans J, Godefroit P (2015) Molecular composition and ultrastructure of Jurassic paravian feathers. Scientific Reports 5: 13520. https://doi.org/10.1038/srep13520

López-Arbarello A, Schröder KM (2014) The species of *Aspidorhynchus* Agassiz, 1833 (Neopterygii, Aspidorhynchiformes) from the Jurassic plattenkalks of southern Germany. Paläontologische Zeitschrift 88: 167–185. https://doi.org/10.1007/s12542-013-0187-z

Lösel P, van de Kamp T, Jayme A, Ershov A, Faragó T, Pichler O, Tan Jerome N, Aadepu N, Bremer S, Chilingaryan S, Heethoff M, Kopmann A, Odar J, Schmelzle S, Zuber M, Wittbrodt J, Baumbach T, Heuveline V (2020) Introducing *Biomedisa* as an open-source online platform for biomedical image segmentation. Nature Communications 11: 5577. https://doi.org/10.1038/s41467-020-19303-w

Maddison WP, Maddison DR (2021) *Mesquite*: a modular system for evolutionary analysis. Version 3.70. http://www.mesquiteproject.org/

Marsh OC (1881) Principal characters of American Jurassic dinosaurs. Part IIX. The order Theropoda. American Journal of Science 27: 329–341. https://doi.org/10.2475/ajs.s3-27.160.329

Mäuser M (1997) Der achte *Archaeopteryx*. Fossilien 14: 156–157. https://doi.org/10.1017/S0790966700003451

Mayr G (2017) Pectoral girdle morphology of Mesozoic birds and the evolution of the avian supracoracoideus muscle. Journal of Ornithology 158: 859–867. https://doi.org/10.1007/s10336-017-1451-x

Mayr G, Pohl B, Hartman S, Peters DS (2007) The tenth skeletal specimen of *Archaeopteryx*. Zoological Journal of the Linnean Society 149: 97–116. https://doi.org/10.1111/j.1096-3642.2006.00245.x

Meyer H von (1857) *Archaeopterix lithographica* (Vogel-Feder) und *Pterodactylus* von Solenhofen. Neues Jahrbuch für Mineralogie, Geognosie, Geologie und Petrefakten-Kunde 1861: 678–679.

Moser M, Rauhut OWM (2011) Der Reusengebiss-Flugsaurier *Ctenochasma*. Fossilien Sonderheft 2011: 47–48.

Mulder EA, Schulp AS, Bijl S, Tafforeau P, Voeten DFAE (2024) A Jurassic early bird: integrative taphonomy and identity of *Ostromia crassipes*. 21st EAVP annual meeting in Longyearbyen (Norway), August 2024, NGF Abstracts and Proceedings, Trondheim, 38 pp.

Niebuhr B, Pürner T (2014) Plattenkalk und Frankendolomit – Lithostratigraphie der Weißjura-Gruppe der Frankenalb (außeralpiner

Oberjura, Bayern). Schriftenreihe der Deutschen Gesellschaft für Geowissenschaften 83: 5–72. https://doi.org/10.1127/sdgg/83/2014/5

Norell MA, Makovicky PJ (1999) Important features of the dromaeosaurid skeleton II: information from newly collected specimens of *Velociraptor mongoliensis*. American Museum Novitates 3282: 1–45.

Olsen AM, Westneat MW (2015) *StereoMorph*: an *R* package for the collection of 3D landmarks and curves using a stereo camera setup. Methods in Ecology and Evolution 6: 351–356. https://doi.org/10.1111/2041-210X.12326

Ooms J (2024) magick: Advanced Graphics and Image-Processing in R. CRAN. https://cran.r-project.org/web/packages/magick/index.html

Ostrom JH (1974) The pectoral girdle and forelimb function of *Deinonychus* (Reptilia: Saurischia): A correction. Postilla 165: 1–11.

Ostrom JH (1976) *Archaeopteryx* and the origin of birds. Biological Journal of the Linnean Society 8: 91–182. https://doi.org/10.1111/j.1095-8312.1976.tb00244.x

Ostrom JH (1978) The osteology of *Compsognathus longipes* Wagner. Zitteliana 4: 73–118.

Pei R, Li Q, Meng Q, Norell MA, Gao K-Q (2017) New specimens of *Anchiornis huxley*i (Theropoda: Paraves) from the Late Jurassic of Northeastern China. Bulletin of the American Museum of Natural History 411: 1–67. https://doi.org/10.1206/0003-0090-411.1.1

Perle A, Norell MA, Clark JM (1999) A new maniraptoran theropod - *Achillobator giganticus* (Dromaeosauridae) - from the Upper Cretaceous of Burkhant, Mongolia. Contributions of the Monogolian-American Paleontological Project 101: 1–105.

Pfeil FH (2011) Ein neues *Asteracanthus*-Gebiss aus den Kieselplattenkalken (Oberjura, Tithonium, Malm Zeta 3, Mörnsheim Formation) des Besuchersteinbruch in Mühlheim. Freunde der Bayerischen Staatssammlung für Paläontologie und Historischer Geologie e.V., Jahresbericht und Mitteilungen 39: 36–60.

Pol D, Escapa IH (2009) Unstable taxa in cladistic analysis: identification and the assessment of relevant characters. Cladistics 25: 515–527. https://doi.org/10.1111/j.1096-0031.2009.00258.x

Pol D, Goloboff PA (2020) The impact of unstable taxa in coelurosaurian phylogeny and resampling support measures for parsimony analyses. Bulletin of the American Museum of Natural History 440: 97–115.

R Core Team (2021) *R*: A language and environment for statistical computing. *R* Foundation for Statistical Computing, Vienna, Austria, https://www.R-project.org

Rauhut OWM (2012) Ein "*Rhamphodactylus*" aus der Mörnsheim-Formation von Mühlheim. Freunde der Bayerischen Staatssammlung für Paläontologie und Historische Geologie e.V., Jahresbericht und Mitteilungen 40: 69–74.

Rauhut OWM, Foth C (2020) The origin of birds: current consensus, controversy, and the occurrence of feathers. In: Foth C, Rauhut OWM (Eds) The Evolution of Feathers. Springer Nature, Cham, 27–45. https://doi.org/10.1007/978-3-030-27223-4_3

Rauhut OWM, Heyng AM, Leonhardt U (2011) Neue Reptilfunde aus der Mörnsheim− Formation von Mülheim. Freunde der Bayerischen Staatssammlung für Paläontologie und Historische Geologie, München 39: 61–71.

Rauhut OWM, Heyng AM, López-Arbarello A, Hecker A (2012) A new rhynchocephalian from the Late Jurassic of Germany with a dentition that is unique amongst tetrapods. PLoS ONE 7: e46839. https://doi.org/10.1371/journal.pone.0046839

Rauhut OWM, López-Arbarello A, Röper M, Rothgaenger M (2017) Vertebrate fossils from the Kimmeridgian of Brunn: the oldest fauna from the Solnhofen Archipelago (Late Jurassic, Bavaria, Germany). Zitteliana 89: 305–329.

Rauhut OWM, Foth C, Tischlinger H (2018) The oldest *Archaeopteryx* (Theropoda: Avialiae): a new specimen from the Kimmeridgian/Tithonian boundary of Schamhaupten, Bavaria. PeerJ 6: e4191. https://doi.org/10.7717/peerj.4191

Rauhut OWM, Tischlinger H, Foth C (2019) A non-archaeopterygid avialan theropod from the Late Jurassic of southern Germany. eLife 8: e43789. https://doi.org/10.7554/eLife.43789

Röper M (2005) East Bavarian plattenkalk – Different types of Upper Kimmeridgian to Lower Tithonian Plattenkalk deposits and facies. Zitteliana B 26: 57–70.

Rowe T, Ketcham RA, Denison C, Colbert M, Xu X, Currie PJ (2001) The *Archaeoraptor* forgery. Nature 410: 539–540. https://doi.org/10.1038/35069145

RStudio Team (2020) *RStudio*: Integrated Development for R. RStudio, PBC, Boston, MA. http://www.rstudio.com/

Russell DA, Dong Z (1993) A nearly complete skeleton of a new troodontid dinosaur from the Early Cretaceous of the Ordos Basin, Inner Mongolia; People's Republic of China. Canadian Journal of Earth Sciences 30: 2163–2173. https://doi.org/10.1139/e93-187

Sanz JL, Pérez-Moreno BP, Chiappe LM, Buscalioni AD (2002) The birds from the Lower Cretaceous of Las Hoyas (Province of Cuenca, Spain). In: Chiappe LM, Witmer LM (Eds) Mesozoic Birds: Above the Heads of Dinosaurs. University of California Press, Berkeley, 209–267.

Schröder KM, López-Arbarello A (2013) Der Schnabelfisch *Aspidorhynchus* aus den Plattenkalken Süddeutschlands. Freunde Der Bayerischen Staatssammlung für Paläontologie und Historische Geologie e.V., Jahresbericht Und Mitteilungen 41: 42–54.

Schwarz, D, E Frey, and C A Meyer. 2007. Novel reconstruction of the orientation of the pectoral girdle in sauropods. The Anatomical Record 290: 32–47. https://doi.org/10.1002/ar.20405

Schweigert G (2007) Ammonite biostratigraphy as a tool for dating Upper Jurassic lithographic limestones from South Germany – first results and open questions. Neues Jahrbuch für Geologie und Paläontologie - Abhandlungen 245: 117–125. https://doi.org/10.1127/0077-7749/2007/0245-0117

Schweigert G (2015) Biostratigraphie der Plattenkalke der südlichen Frankenalb. In: Arratia G, Schultze H-P, Tischlinger H, Viohl G. (Eds) Solnhofen – Ein Fenster in die Jurazeit. Verlag Dr. Friedrich Pfeil, München, 63–66.

Sereno PC (1999) The evolution of dinosaurs. Science 284: 2137–2147. https://doi.org/10.1126/science.284.5423.2137

Šlenker M, Koutecký P, Marhold K (2022) *MorphoTools2*: an *R* package for multivariate morphometric analysis. Bioinformatics 38: 2954–2955. https://doi.org/10.1093/bioinformatics/btac173

Slowikowski K (2024) *ggrepel*: Automatically position non-overlapping text labels with '*ggplot2*'. https://ggrepel.slowkow.com/, https://github.com/slowkow/ggrepel

Stone R (2010) Bird-dinosaurier link formed up, and in brilliant technicolor. Science 327: 508. https://doi.org/10.1126/science.327.5965.508

Tischlinger H (2001) Die oberjurassischen Plattenkalke von Daiting. In: Weidert WK (Ed) Klassische Fundstellen der Paläontologie, Bd. IV. Goldschneck Verlag, Korb, 139–151.

Tischlinger H (2009) Der achte *Archaeopteryx* - das Daitinger Exemplar. Archaeopteryx 27: 1–20.

Turner AH, Makovicky PJ, Norell MA (2012) A review of dromaeosaurid systematics and paravian phylogeny. Bulletin of the American Museum of Natural History 371: 1–206. https://doi.org/10.1206/748.1

Viohl G (2015) Der geologische Rahmen: die Südliche Frankenalb und ihre Entwicklung. In: Arratia G, Schultze H-P, Tischlinger H, Viohl G (Eds) Solnhofen – Ein Fenster in die Jurazeit. Verlag Dr. Friedrich Pfeil, München, 56–62.

Viohl G, Zapp M (2007) Schamhaupten, an outstanding Fossil-Lagerstätte in a silicified Plattenkalk around the Kimmeridgian-Tithonian boundary (Southern Franconian Alb, Bavaria). Neues Jahrbuch für Geologie und Paläontologie - Abhandlungen 245: 127–142. https://doi.org/10.1127/0077-7749/2007/0245-0127

Voeten DFAE, Cubo J, de Margerie E, Röper M, Beyrand V, Bures S, Tafforeau P, Sanches S (2018) Wing bone geometry reveals active flight in *Archaeopteryx*. Nature Communications 9: 283. https://doi.org/10.1038/s41467-018-03296-8

Voeten, DF E, van Bijlert PA, Tafforeau P, Schulp AS (2024) Reimagining *Archaeopteryx*: unlocking the 3D anatomy of incipient dinosaur flight. 21st EAVP annual meeting in Longyearbyen (Norway), August 2024, NGF Abstracts and Proceedings, Trondheim, 61 pp.

Wallaard JJW, van Bakel BWM, Fraaije RHB, Jagt JWM (2021) A new primitive crab from the Upper Jurassic plattenkalks of the Solnhofen Archipelago (southern Germany). Neues Jahrbuch für Geologie und Paläontologie, Abhandlungen 302: 131–138. https://doi.org/10.1127/njgpa/2021/1023

Wang X, Pittman M, Zheng X, Kaye TG, Falk AR, Hartman S, Xu X (2017) Basal paravian functional anatomy illuminated by high-detail body outline. Nature Communications 8: 14576. https://doi.org/10.1038/ncomms14576

Wang M, O'Connor JK, Zhou Z (2019a) A taxonomical revision of the Confuciusornithiformes (Aves: Pygostylia). Vertebrata PalAsiatica 57: 1–37.

Wang M, O'Connor JK, Xu X, Zhou Z (2019b) A new Jurassic scansoriopterygid and the loss of membranous wings in theropod dinosaurs. Nature 569: 256–259.

Wellnhofer P (2009) *Archaeopteryx*: The Icon of Evolution. Verlag Dr. Friedrich Pfeil, München, 208 pp.

Wickham H (2016) *ggplot2*: Elegant Graphics for Data Analysis. Springer, Cham, 260 pp. https://doi.org/10.1007/978-3-319-24277-4_9

Wickham H, Henry L, Pedersen T, Luciani T, Decorde M, Lise V (2023) *svglite*: An 'SVG' graphics device. *R* package version 2.1.3.9000. https://github.com/r-lib/svglite, https://svglite.r-lib.org

Wilke C (2024) *cowplot*: Streamlined plot theme and plot annotations for *'ggplot2'*. *R* package version 1.1.3. https://wilkelab.org/cowplot/

Wilkinson M (1994) Common cladistic information and its consensus representation: reduced Adams and reduced cladistic consensus trees and profiles. Systematic Biology 43: 343–368. https://doi.org/10.1093/sysbio/43.3.343

Xu L, Wang M, Chen R, Dong L, Lin M, Xu X, Tang J, You H, Zhou G, Wang L, He W, Li Y, Zhang C, Zhou Z (2023) A new avialan theropod from an emerging Jurassic terrestrial fauna. Nature 621: 336–343. https://doi.org/10.1038/s41586-023-06513-7

Xu X, Norell MA (2004) A new troodontid dinosaur from China with avian-like sleeping posture. Nature 431: 838–841. https://doi.org/10.1038/nature02898

Xu X, Norell MA, Wang X, Makovicky PJ, Wu X (2002) A basal troodontid from the Early Cretaceous of China. Nature 415: 780–784. https://doi.org/10.1038/415780a

Xu X, Zhao Q, Norell MA, Sullivan C, Hone DWE, Erickson GM, Wang X, Han F, Guo Y (2009) A new feathered maniraptoran dinosaur fossil that fills a morphological gap in avian origin. Chinese Science Bulletin 54: 430–435. https://doi.org/10.1007/s11434-009-0009-6

Xu X, You H, Du K, Han F (2011) An *Archaeopteryx*-like theropod from China and the origin of Avialae. Nature 475: 465–470. https://doi.org/10.1038/nature10288

Xu X, Zheng X, Sullivan C, Wang X, Xing L, Wang Y, Zhang X, O'Connor JK, Zhang F, Pan Y (2015) A bizarre Jurassic maniraptoran theropod with preserved evidence of membranous wings. Nature 521: 70–73. https://doi.org/10.1038/nature14423

Xu X, Zhou Z, Sullivan C, Wang Y, Ren D (2016) An updated review of the Middle-Late Jurassic Yanliao Biota: chronology, taphonomy, paleontology and paleoecology. Acta Geologica Sinica - English Edition 90: 2229–2243. https://doi.org/10.1111/1755-6724.13033

Zanno LE (2010) A taxonomic and phylogenetic review of Therizinosauria. Journal of Systematic Palaeontology 8: 503–543. https://doi.org/10.1080/14772019.2010.488045

Zelditch M, Swiderski D, Sheets HD (2012) Geometric Morphometrics for Biologists: a Primer. Academic Press, 488 pp.

Zheng X, Wang X, Sullivan C, Zhang X, Zhang F, Wang Y, Li F, Xu X (2018) Exceptional dinosaur fossils reveal early origin of avian-style digestion. Scientific Reports 8: 14217. https://doi.org/10.1038/s41598-018-32202-x

Zhou Z, Zhang F (2002) Largest bird from the Early Cretaceous and its implications for the earliest avian ecological diversification. Naturwissenschaften 89: 34–38. https://doi.org/10.1007/s00114-001-0276-9

Zhou Z, Zang FC (2006) A beaked basal ornithurine bird (Aves, Ornithurae) from the Lower Cretaceous of China. Zoologica Scripta 35: 363–373. https://doi.org/10.1111/j.1463-6409.2006.00234.x

Supplementary material 1

List of specimens included in the GMM analysis

Authors: Christian Foth, Thomas van de Kamp, Helmut Tischlinger, Theron Kantelis, Ryan M. Carney, Marcus Zuber, Elias Hamann, Jonathan J. W. Wallaard, Norbert Lenz, Oliver W. M. Rauhut, Eberhard Frey

Data type: pdf

Link: https://doi.org/10.3897/fr.28.131671.suppl1

Supplementary material 2

Nexus file, including the data matrix and the strict and reduced consensus trees from the phylogenetic analyses

Authors: Christian Foth, Thomas van de Kamp, Helmut Tischlinger, Theron Kantelis, Ryan M. Carney, Marcus Zuber, Elias Hamann, Jonathan J. W. Wallaard, Norbert Lenz, Oliver W. M. Rauhut, Eberhard Frey
Data type: nex

Link: https://doi.org/10.3897/fr.28.131671.suppl2

Supplementary material 3

Character list and reduces consensus trees with bootstrap values

Authors: Christian Foth, Thomas van de Kamp, Helmut Tischlinger, Theron Kantelis, Ryan M. Carney, Marcus Zuber, Elias Hamann, Jonathan J. W. Wallaard, Norbert Lenz, Oliver W. M. Rauhut, Eberhard Frey
Data type: pdf

Link: https://doi.org/10.3897/fr.28.131671.suppl3

Supplementary material 4

Data matrix for TNT

Authors: Christian Foth, Thomas van de Kamp, Helmut Tischlinger, Theron Kantelis, Ryan M. Carney, Marcus Zuber, Elias Hamann, Jonathan J. W. Wallaard, Norbert Lenz, Oliver W. M. Rauhut, Eberhard Frey
Data type: tnt

Link: https://doi.org/10.3897/fr.28.131671.suppl4

Supplementary material 5

3D model of SMNK PAL 10,000

Authors: Christian Foth, Thomas van de Kamp, Helmut Tischlinger, Theron Kantelis, Ryan M. Carney, Marcus Zuber, Elias Hamann, Jonathan J. W. Wallaard, Norbert Lenz, Oliver W. M. Rauhut, Eberhard Frey
Data type: pdf

Link: https://doi.org/10.3897/fr.28.131671.suppl5